ANALYTICAL MODELING OF CHANNEL POTENTIAL AND THRESHOLD VOLTAGE OF TRIPLE MATERIAL GATE AlGaN/GaN HEMT AND STUDY OF ITS SELF-HEATING EFFECT

A thesis submitted to

the Department of Electrical and Electronic Engineering

of

Bangladesh University of Engineering and Technology

in partial fulfillment of the requirements

for the degree of

MASTER OF SCIENCE IN ELECTRICAL AND ELECTRONIC ENGINEERING

By,

MD. TASHFIQ BIN KASHEM

Student ID: 0412062243 F

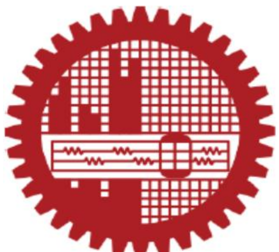

BANGLADESH UNIVERSITY OF ENGINEERING AND TECHNOLOGY

August' 2016

DECLARATION

It is hereby declared that this thesis or any part of it has not been submitted elsewhere for the award of any degree or diploma.

(Md. Tashfiq Bin Kashem)

DEDICATION

I would like to dedicate this work to my parents who have always been caring and supportive to me.

APPROVAL CERTIFICATE

The thesis titled "ANALYTICAL MODELING OF CHANNEL POTENTIAL AND THRESHOLD VOLTAGE OF TRIPLE MATERIAL GATE AlGaN/GaN HEMT AND STUDY OF ITS SELF-HEATING EFFECT" submitted by Md. Tashfiq Bin Kashem, Student ID: 0412062243F, Session: April 2012 has been accepted as satisfactory in partial fulfillment of the requirement for the degree of MASTER OF SCIENCE IN ELECTRICAL AND ELECTRONIC ENGINEERING on 8th August, 2016.

BOARD OF EXAMINERS

1. ______________________________ Chairman

Dr. Samia Subrina
Associate Professor, Supervisor
Department of EEE, Bangladesh University of Engineering and Technology,
Dhaka-1205.

2. ______________________________ Member

Dr. Quazi Deen Mohd Khosru
Professor and Head, (Ex-Officio)
Department of EEE, Bangladesh University of Engineering and Technology,
Dhaka-1205.

3. ______________________________ Member

Dr. Md. Ziaur Rahman Khan
Professor,
Department of EEE, Bangladesh University of Engineering and Technology,
Dhaka-1205.

4. ______________________________ Member

Dr. Muhibul Haque Bhuyan
Professor and Chairman, External
Department of Electrical and Electronic Engineering, Southeast University,
251/A & 252, Tejgaon Industrial Area, Dhaka-1208.

TABLE OF CONTENTS

List of Figures			**ix**
List of Tables			**xi**
List of Symbols			**xii**
List of Abbreviations			**xiv**
Acknowledgement			**xv**
Abstract			**xvi**
Chapter 1		**Introduction**	**1-9**
1.1		Literature Review	3
1.2		Objectives of the Work	7
1.3		Thesis Outline	8
Chapter 2		**Theoretical Background**	**10-20**
2.1		Material Properties of GaN	10-12
	2.1.1	Structural Properties	10
	2.1.2	Electrical Properties	11
2.2		AlGaN/GaN HEMT	12-20
	2.2.1	Device Structure	12
	2.2.2	Polarization	13-15
	2.2.2.1	Spontaneous Polarization	13
	2.2.2.2	Piezoelectric Polarization	13
	2.2.3	Formation of Two Dimensional Electron Gas (2DEG)	15
	2.2.4	Trapping Effect	17

	2.2.5	Thermal Properties	18
	2.2.6	Applications	20
Chapter 3		**Analytical Modeling of Proposed Device**	**21-32**
3.1		Device Structure	21
3.2		Channel Potential	22
3.3		Electric Field	28
3.4		Minimum Channel Potential	29
3.5		Threshold Voltage	30
3.6		Simulation Methodology	32
Chapter 4		**Thermal Modeling**	**33-34**
4.1		Self-Heating Issue in AlGaN/GaN HEMT	33
4.2		Thermal Modeling	33
Chapter 5		**Results and Discussion**	**35-56**
5.1		Channel Potential along the Channel	36-43
	5.1.1	Comparison among Various Device Structures	36
	5.1.2	Effect of Ratio of Individual Metal Gate Length	36
	5.1.3	Variation with Total Channel Length	37
	5.1.4	Effect of Drain Bias	38
	5.1.5	Variation with Barrier Layer Doping Concentration	39
	5.1.6	Changes with Mole Fraction of Al in AlGaN	40

	5.1.7	Effect of Barrier Layer Thickness	40
	5.1.8	Minimum Channel Potential: Impact of Total Channel Length	41
	5.1.9	Polarization Effect	42
	5.1.10	Effect of Trapped Charge	43
5.2		Electric Field along the Channel	43-46
	5.2.1	Comparison among Various Device Structures	43
	5.2.2	Effect of Ratio of Individual Metal Gate Length	44
	5.2.3	Effect of Ratio of Individual Metal Gate Length	45
	5.2.4	Effect of Ratio of Individual Metal Gate Length	46
5.3		Threshold Voltage	46-50
	5.3.1	Effect of Barrier Layer Thickness	46
	5.3.2	Variation with Total Channel Length	47
	5.3.3	Changes with Ratio of Individual Metal Gate Length	48
	5.3.4	Effect of Drain Bias	49
	5.3.5	Comparison among Various Device Structures	49
5.4		Drain Induce Barrier Lowering (DIBL) Effect	50-52
	5.4.1	Comparison among Various Device Structures	50
	5.4.2	Influence of Ratio of Individual Metal Gate Length	51
5.5		Channel Temperature Due to Self-Heating Effect	52-56
	5.5.1	Temperature Profile across the Device: Comparison among Various Device Structures	52

5.5.2	Effect of Drain and Gate Biases	53
5.5.3	Effect of AlGaN Layer Thickness	54
5.5.4	Impact of Ratio of Different Gate Metal Length	55
5.5.5	Comparison Among Various Substrate Materials	55
Chapter 6	**Conclusion**	**57-58**
6.1	Conclusion	57
6.2	Scopes of Future Work	58
References		**59-64**

LIST OF FIGURES

Fig. 2.1	The Wurtzite structure of GaN (Figure is adopted from Ref. [40])	10
Fig. 2.2	Stick and Ball representation of the tetrahedral arrangement of Ga and N (Figure is adopted from Ref. [54])	14
Fig. 2.3	Spontaneous and piezoelectric polarization field induced charges in AlGaN/GaN HEMT	15
Fig. 2.4	Conduction band energy band diagram of AlGaN/GaN heterostructure (adopted from [56])	15
Fig. 2.5	Possible location of trap states in AlGaN/GaN HEMT	17
Fig 3.1	Two dimensional schematic diagram of Triple Material Gate $Al_{0.3}Ga_{0.7}N$/GaN HEMT	21
Fig. 5.1.1	Channel potential distribution along the channel position for SMG, DMG and TMG HEMT at V_{gs} = -0.2V, V_{ds} = 0.2V, L_1:L_2:L_3 = 1:1:1 for TMG HEMT	36
Fig. 5.1.2	Channel potential profile of TMG HEMT along the position of the channel for various metal gate length (L_1, L_2 and L_3) ratios	37
Fig. 5.1.3	Variation in channel potential with the channel position for different values of total channel lengths considering L_1:L_2:L_3 = 1:1:1	38
Fig. 5.1.4	Channel potential variation with channel position for different drain to source voltages	38
Fig. 5.1.5	Change in channel potential with lateral position along the channel for various doping concentration of donor atoms	39
Fig. 5.1.6	Variation in channel potential profile versus lateral position along the channel for different mole fraction values of Al in AlGaN	40
Fig. 5.1.7	Shift of channel potential with lateral position along the channel for different thickness of AlGaN barrier layer	41
Fig. 5.1.8	Minimum channel potential against total channel length for different drain to source voltages	41
Fig. 5.1.9	Channel potential as a function of lateral position along the channel with and without polarization effect	42

Fig. 5.1.10 Channel potential profile along channel position with different trap charge 43

Fig. 5.2.1 Variation in electric field with lateral position of the channel for SMG, DMG and TMG HEMT 44

Fig. 5.2.2 Electric field variation with position along the channel of TMG HEMT for different ratio of L_1, L_2 and L_3 45

Fig. 5.2.3 Electric field profile along channel position for different drain to source Voltages 45

Fig. 5.2.4 Effect of polarization on electric field distribution along the channel 46

Fig. 5.3.1 Threshold voltage variation of TMG HEMT with lateral position along the channel for different values of t_b 47

Fig. 5.3.2 Threshold voltage distribution with drain to source voltage for various total channel lengths 48

Fig. 5.3.3 Threshold voltage versus total channel length for different metal gate length ratios 48

Fig. 5.3.4 Variation in threshold voltage with total channel length for various drain to source voltages 49

Fig. 5.3.5 Change in threshold voltage with total channel length for DMG and TMG HEMT 50

Fig. 5.4.1 DIBL vs total channel length for DMG and TMG HEMT structures 51

Fig. 5.4.2 Impact of different ratio of L_1, L_2 and L_3 on DIBL effect in TMG HEMT for various total channel lengths 52

Fig. 5.5.1 Temperature distribution profile across the device for TMG HEMT 53

Fig. 5.5.2 Maximum temperature in TMG HEMT vs drain to source voltage, V_{ds} for different gate to source voltages, V_{gs} 54

Fig. 5.5.3 Maximum channel temperature versus AlGaN layer thickness 54

Fig. 5.5.4 Effect of ratio of gate metal lengths on maximum channel temperature 55

Fig. 5.5.5 Maximum channel temperature for various substrate materials 56

LIST OF TABLES

Table 2.1	Material properties of various semiconductor materials	12
Table 2.2	Thermal conductivities of familiar substrate materials	19
Table 4.1	Electrical and thermal conductivity of different materials used in thermal simulation	34
Table 5.1	Model parameters	35
Table 5.2	Maximum channel temperature for TMG, DMG and SMG HEMT	53

LIST OF SYMBOLS

Symbol	Meaning
C_{13}, C_{33}	Elastic constant parameters
d	Lattice constant parameter
e_{33}, e_{33}	Piezoelectric constants
E	Electric field
$E_{g,Al_mGa_{1-m}N}$	Energy bandgap of AlGaN
$E_{g,GaN}$	Energy bandgap of GaN
E_{he}	Electric field at the hetero interface
ΔE_c	Conduction band offset at the AlGaN/GaN interface
J	Electric current density
k	Thermal conductivity
k_B	Boltzmann constant
L	Total channel length
L_1, L_2 and L_3	Length of the three gate metals
m	Al mole fraction in AlGaN
N_D	Impurity density of AlGaN barrier layer
N_i	Intrinsic carrier concentration
N_{si}	Sheet carrier concentration in the 2DEG channel
N_{tr}	Net charged traps per unit area
$P_{piezo}(Al_mGa_{1-m}N)$	Sheet carrier density induced by piezoelectric polarization of AlGaN
$P_{spon}(Al_mGa_{1-m}N)$	Sheet carrier density induced by spontaneous polarization of AlGaN
$P_{spon}(GaN)$	Sheet carrier density induced by spontaneous polarization of GaN
Q	Resistive heat
q	Electron charge
T	Temperature

t_b	AlGaN Barrier layer thickness
t_s	AlGaN Spacer layer thickness
t	Total AlGaN layer thickness
x_{min}	Minimum channel potential location
V_o	Voltage required to annihilate 2DEG
V_{ds}	Drain to source voltage
V_{FB}	Flat band voltage
V_{gs}	Gate to source voltage
V_{th}	Threshold voltage
V_T	Thermal voltage
ε_s	Permittivity of AlGaN
Φ	Electrostatic potential
Φ_a	Work function of AlGaN
Φ_{bi}	Built in voltage
Φ_c	Channel potential
Φ_f	Fermi potential
Φ_{M1}, Φ_{M2} and Φ_{M3}	Work functions of the three materials in the gate electrode
Φ_{sb}	Schottky barrier height
χ_a	Electron affinity of AlGaN
δ_{GaN}	Electron-phonon coupling constant
τ_{GaN}	Average phonon temperature
σ_{pol}	Polarization induced sheet charge density
ρ	Electric resistivity
σ	Electric conductivity

LIST OF ABBREVIATIONS

Abbreviation	Full Form
AlGaN	Aluminium Gallium Nitride
DIBL	Drain Induced Barrier Lowering
DMG	Dual Material Gate
GaN	Gallium Nitride
HEMT	High Electron Mobility Transistor
SCE	Short Channel Effect
SiC	Silicon Carbide
SMG	Single Material Gate
TMG	Triple Material Gate
2DEG	Two Dimensional Electron Gas

ACKNOWLEDGEMENT

I would like to express my sincere indebtedness to my thesis supervisor, Dr. Samia Subrina, Associate Professor, Department of Electrical and Electronic Engineering, Bangladesh University of Engineering and Technology, for her insightful suggestions, guidance and support throughout the thesis work. She inspired me to chase the desperate problems with patience and knowledge. It is because of her perceptive guidance and instructions, I have been able to complete the thesis work.

Thanks to my family members, well-wishers and friends who helped in various ways to complete the work. I would like to express my heartiest gratitude to my parents for whom I am standing at this position.

ABSTRACT

AlGaN/GaN based high electron mobility transistors (HEMTs) are rapidly progressing towards becoming prime candidate for high power, high frequency and high temperature electronics applications and the reason is having several outstanding and unique electrical properties like large energy band gap, high electron mobility, high saturation velocity, low thermal impedance and high breakdown field. Device dimensions of HEMTs are being continuously scaled down with the advancement of ultra large scale integration (ULSI) and very large scale integration (VLSI) technology for achieving high speed, high packing density and improved performance. This continual downscaling has invoked dominance of several short channel effects (SCEs) because of reduced gate controllability over the channel and resulted in poor carrier transport efficiency and degraded performance. Numerous new architectures have been developed to diminish these SCEs. Gate material engineering technique in which the gate electrode is composed of more than one material with different work function has been adopted by many devices to acquire better SCE handling capability. In the triple material gate HEMT, the gate electrode is formed by fabricating three materials with different work functions laterally. The work function of the material near the source is the highest and that near the drain end is the lowest. The high work function near the source results in enhanced carrier transport efficiency due to quick acceleration of carriers in the channel and the low work function near the drain leads to decrease in electric field peak at the drain end and reduction of hot carrier effect. Moreover, two screen gates screen the effect of drain potential on the source-channel barrier and suppress drain induced barrier lowering (DIBL) effect. In this work, a two dimensional analytical model of channel potential, electric field and threshold voltage of triple material gate (TMG) AlGaN/GaN HEMT has been developed. Two dimensional Poisson's equation with suitable boundary conditions has been solved to derive the channel potential using parabolic approximation method. Spontaneous and piezoelectric polarization induced charges at the AlGaN/GaN interface have been incorporated in the model. Effect of traps produced due to process defects during device growth has been analyzed. The device performance has been explored with the variation in various device parameters like total channel length, ratio of length of different gate metals, barrier layer thickness etc. and compared with single material gate and dual material gate HEMT structures. Superior performance of TMG HEMT over other device structures has been found in terms of reduction of SCEs and enhanced carrier velocity. Results from the proposed analytical model have been validated against the data obtained from

a commercially available numerical device simulator. Moreover, proper investigation of self-heating effect is necessary in GaN-based HEMT devices as this significantly impacts device performance and reliability. Therefore, a simulation model has been developed in this work to explore the self-heating effect of the proposed device structure. Temperature distribution profile across the device has been obtained and effects of different device parameters and bias voltages on maximum operating channel temperature have been demonstrated.

CHAPTER ONE

INTRODUCTION

High Electron Mobility Transistor (HEMT), having several attractive features like high carrier mobility, large breakdown voltage, reduced impurity scattering, high sheet charge density and efficient thermal transport, have become a dominant choice among transistors to be used in high frequency, high temperature and high power applications [1-5]. A two dimensional electron gas (2DEG) channel, formed at the heterointerface of wide and comparatively narrow bandgap materials, acts as basis for operation of HEMT. Large amount of sheet carrier concentration generated at the 2DEG channel paves the way for having copious exciting features and ensures superior performance of HEMT over other devices. Nitride based devices such as AlGaN/GaN HEMTs are proved to provide much more efficient operation over other HEMT devices because of having high peak electron drift velocity and large critical electric field. These result in increased breakdown voltage, large scale current density and enhanced power density [2]. High conduction band offset between AlGaN and GaN and a high carrier concentration in 2DEG channel without any kind of deliberate doping, just due to the presence of strong spontaneous and piezoelectric polarization effects [6] have made AlGaN/GaN HEMT an attractive device among other nitride based hetero structures for wireless BTS applications, radar and satellite communication services [7-9]. Continuous downscaling of HEMT to incorporate ULSI and VLSI technology has intensified device performance degradation problems. Reduced control of gate over the channel resulting from scaling down the devices into nanometer regime gives rise to the short channel effects (SCEs) like hot carrier effect, drain induced barrier lowering (DIBL), threshold voltage shift [10] etc. which ultimately deteriorates device performance and quality. Observing this concerned effect and for further downscaling of the device, several techniques have already been taken to lessen SCEs and abate the problems arising from this. Gate engineering approach is considered to be one of the most efficient techniques in this regard in which the gate terminal is composed of more than one material with different work functions connected side-by-side. In such structure, the metal gate with the highest work function is called the control gate while the other metal gates are known as screen gates. This methodology was first implemented for MOSFET by Long *et al.* [11] in which two different metals were used to form the gate contact and thus the structure

was named as Dual Material Gate MOSFET (DMG MOSFET). This device provides less amount of drain control and ensures more gate controllability over the channel by forming a step function shaped surface potential distribution. Later on, Kumar *et al.* implemented the technique in HEMT and proposed a device named DMG HEMT [12]. DMG HEMT provides enhanced average carrier velocity by introducing the gate metal with higher work function near the source as well as reduced peak electric field at the drain end owing to placement of gate material with lower work function near the drain terminal.

Recently, after further modification of DMG MOSFET, a new structure titled as Triple Material Gate MOSFET (TMG MOSFET) device has been proposed where three metals with varying work functions were employed to form the gate contact. Various theoretical, experimental and simulation studies with this structure have revealed its better performance with respect to DMG MOSFET in terms of mitigation of SCEs and providing high carrier velocity [13-16]. More steps in surface potential and electric field profile in TMG MOSFET compared to DMG MOSFET accounts for improved screening of the effects of drain voltage over the channel and much more weakened hot carrier effect. TMG technique has also been exploited for tunnel FET and FinFET [17, 18]. But till now, no analytical model has been reported to investigate the outcome of implementing TMG structure technique for AlGaN/GaN HEMTs. Furthermore, along with electrical characteristics, proper study of thermal performance of the device is equally important to utilize the structure in numerous high temperature and high power applications. Self-heating effect, associated with the device operation at high power density level, is responsible for diminishing electron mobility due to enhanced phonon scattering and thus reducing device efficiency. Average temperature rise and non-uniform distribution of dissipated power, leading to the formation of hotspots near device channels, result in degradation of the drain current, gain and output power, increase in gate-leakage current and poor reliability. Therefore, for device optimization, it is important to study the self-heating effects in AlGaN/GaN HEMTs considering different aspects. No model has been developed yet to examine the self-heating effects in DMG and TMG AlGaN/GaN HEMTs.

In this work, an analytical model has been developed to determine channel potential profile, electric field distribution and threshold voltage of TMG AlGaN/GaN HEMT. The model is built up by solving the two dimensional Poisson's equation using parabolic approximation procedure along with required boundary conditions. Both spontaneous and piezoelectric

polarization effects and temperature and mole fraction dependence of different device parameters have been taken into consideration to properly perform the formulation and describe the device characteristics. Effect of trapped charge formed during device fabrication will be analyzed for more realistic modeling of the device. Impact of changing various device parameters on analytically determined profiles has been examined thoroughly and comparison with Single Material Gate (SMG) HEMT and DMG HEMT is also performed to identify the most efficient device in terms of speed and performance parameters. A simulation model has also been established for this structure using 2D device simulator. The results obtained from both analytical and simulation models have been compared to validate our proposed model. Quantum Mechanical Effect (QME) and ballistic transport phenomena have not been considered in this study as the channel length of the proposed device structure is taken to be long enough to ignore these effects. Temperature rise across the proposed device arising from self-heating effect has been explored by building up a simulation framework and effect of various parameters on temperature profile has been investigated.

1.1 Literature Review

Khan *et al*. [19] have first explored AlGaN/GaN HEMT and reported its high-frequency characterization. Superior values of cutoff frequency and maximum oscillation frequency were found in comparison to FETs, based on other wide band gap semiconductor materials. Later, various researches have been performed to investigate polarization phenomenon and trapping effect associated with the device.

Polarization works as a unique feature and plays a vital role in the formation of 2DEG at the hetero interface in AlGaN/GaN HEMTs. A number of researches have been explored to explain the polarization phenomenon and its impact on device characteristics [20-24]. Ambacher *et al.* [20] have studied the formation of 2DEG induced by spontaneous and piezoelectric polarization in AlGaN/GaN heterostructures. They have reported analytical expressions and calculated polarization induced sheet charge and sheet carrier concentration. Kumar *et al.* [21] have investigated the effect of spontaneous and strain dependent piezoelectric polarization in 2D analytical model of single material gate AlGaN/GaN HEMT and found current voltage characteristics and small signal parameters. Kumar *et al.* [22] have incorporated spontaneous and piezoelectric polarization induced charges in the analytical model using accurate velocity field relationship to predict the dc and microwave performance of AlGaN/GaN modulation

doped field effect transistor (MODFET). High current level, high cutoff frequency and large transconductance values have been obtained in their study. Asbeck *et al.* [23] have performed experimental study to estimate piezoelectric charge density at (0001) AlGaN/GaN interfaces of undoped HFET structures grown by both MBE and MOCVD. It has been observed that sheet carrier concentration increases with the increase in mole fraction of Al in AlGaN. Lenka *et al.* [24] have investigated 2DEG transport properties of the charge carriers of AlGaN/GaN and AlGaAs/GaAs HEMT structures considering spontaneous and piezoelectrical polarization effects and various subbands in the 2DEG. In this work, conduction band profile and subband structure of AlGaN/GaN HEMT have been calculated by a self-consistent numerical method and a sharp 2DEG has been found.

Furthermore, effect of traps in different layers formed from various defects during device growth have been investigated in multiple research works [25-29]. Zhang *et al.*[25] have explored the effects of the AlGaN/GaN interface traps on the transient response of AlGaN/GaN HEMT by dint of experimental works and numerical simulation. Analysis of the drain current stimulated by the gate and drain turn on voltage pulses has been performed to identify the influence of the trapped charges. Tirado *et al.* [26] have investigated the impact of the surface trap on the transient response of AlGaN/GaN HEMTs. Drain current dispersion effect along with gate-lag and drain-lag turn on measurements have been examined when gate and drain voltage pulses were applied. Bradley *et al.* [27] have identified the defects in each layer of AlGaN/GaN HEMT using low energy electron excited nanoscale luminescence spectroscopy (LEEN) and correlated their effect on two-dimensional electron gas (2DEG) confinement. AlGaN/GaN heterostructures with different electrical properties have been investigated using incident electron beam energies of 0.5 to 15keV to probe electronic state transitions within each layer of the heterostructure. Klein *et al.* [28] have utilized photoionization spectroscopy technique to characterize and identify trap centers causing current collapse in AlGaN/GaN HEMT grown by metal organic chemical vapour deposition (MOCVD) process. Binari *et al.* [29] have explored buffer and surface trapping effects, on microwave power performance of AlGaN/GaN HEMT.

Various methodologies have been undertaken to examine the influence of self-heating effect which occurs because of collisional energy loss from electrons to the crystal and limits high power high frequency performance of AlGaN/GaN HEMTs [30-34]. Chattopadhyay [30] has presented a physics based unified analytical model describing the relationship of self-heating

effect with device structure and channel current. Hosch*et al.* [31] have investigated effect of self-heating in high power AlGaN/GaN HEMT by performing Micro-Raman thermography measurements to obtain the device temperature at various power and voltage levels. They observed the influence of drain voltage on temperature distribution of the device while the dissipated power was kept constant by applying a gate bias. The results were further investigated and explained through numerical electro-thermal device simulations. Ahmad *et al.* [32] have developed UV-Raman spectroscopy to determine the temperature distribution profile in AlGaN/GaN HFET for various drain and gate voltages. Measurements were carried out using micro-Raman scattering excited by above band gap ultraviolet and below band gap visible laser light. Ultraviolet excitation probes the GaN near the AlGaN/GaN interface of the device where 2DEG carries the source-drain current. The experimental results were verified by electrical and thermal simulations. Gaska *et al.* [33] have studied comparative analysis of self-heating effects in AlGaN/GaN HFETs grown on conducting 6H-SiC and insulating sapphire substrates using experimental measurements. Self-heating kinetics and characteristics heating times have been investigated in that study. It has been demonstrated that AlGaN/GaN HFETs grown on SiC substrate provide superior electron transport properties along with excellent thermal properties. Wu *et al.* [34] have examined the effect of self-heating on current, power and temperature profile under pulsed and DC conditions. Self-heating effects were found to be significant even for very short pulse widths as hot phonons or non-equilibrium phonons might cause current (electron velocity) suppression for short pulses.

The scaling of HEMTs into micrometer and sub micrometer range for achieving high speed operation has intensified several short channel effects and as a result, numerous studies have been performed to explain the drawbacks arising from short channel effects and approaches have been taken to counteract the problems [10, 35-39]. Awano *et al*. [35] have reported electron transport and high speed performance measurements of quarter micrometer gate AlGaAs/GaAs HEMT by fabricating the device as well as by accomplishing two dimensional Monte Carlo simulation. The simulation was performed by calculation of electron transport simultaneously with the Monte Carlo method and Poisson's equation and shorter room temperature propagation delay, high transconductance and high unity current gain cutoff frequency have been found. But gate lengths of the devices have been shrunken more afterwards and then SCEs have become prominent with this structure and ultimately performance degraded. Then the same group [10] has performed Monte Carlo simulation and

experiment to investigate short channel effects of subquarter micrometer gate HEMTs. Effect of aspect ratio of the channel on HEMT performance has been discussed. Chen *et al*. [36] have lifted up the improvement in diminishing short channel effects (SCEs) of AlGaN/GaN MODFETs by using dual gate structure. SCEs are minimized due to screening of the drain voltage by application of dc bias at the second gate and both high cut off frequency and large breakdown field are obtained. Yet, carrier transport efficiency dependent on electric field distribution along the channel does not improve in this structure. Palacios *et al*. [37] have studied the effect of using a back barrier to the electrons in deep submicrometer gate length GaN/ultrathin InGaN/GaN heterojunction. Electric field induced by polarization in the InGaN layer elevates the conduction band in the GaN buffer over the 2DEG channel and increase the confinement of the 2DEG. Thus significant improvement in output conductance and pinch off voltage have been found because of the enhanced modulation efficiency of the electrons in the channel. Shur [38] has presented an analytical model of split gate FET (SFET) structure for short channel AlGaAs/GaAs HEMT. Two closely spaced gates exist in split gate structures and a more positive gate voltage is applied to the gate closer to the drain end. This leads to higher electric field under the gate that is nearer to the source and causes a prompt increase in electron velocity. As a result, increased average carrier velocity and faster carrier transport are obtained. Ismail *et al*. [39] have utilized the split gate FET approach for a shorter gate length AlGaAs/GaAs HEMT. The structure provides enhanced controllability of threshold voltage and reduced short channel effects. However, high speed performance is hampered in split gate structure due to inherent fringing capacitance between the gates.

Gate material engineering technique, i.e. use of more than one material to form the gate electrode in order to reduce SCEs and achieve high efficiency have been reported in various literatures. Some works focused on Dual Material Gate (DMG) structure [11,12] while recently, researchers have dealt with Triple Material Gate (TMG) structure for different FETs. [13,14,17,18] Long *et al.* [11] have carried out experimental study and numerical simulation to examine the performance of dual material gate (DMG) HFET device in which two laterally connected materials with different work functions formed the gate terminal. The work function of the gate material near the source end is greater than that of the gate metal near the drain end to make the threshold voltage near the source higher than the drain. As a consequence, charge carriers accelerate quickly in the channel and carrier transport efficiency has been improved. SCEs also get reduced due to having steps in the channel potential. Kumar *et al.* [12] have

developed a 2-D analytical model for channel potential and electric field of DMG AlGaN/GaN HEMT. It has been shown that drain potential variations are screened by the gate near the drain end because of the step function in channel potential profile produced by the difference in work functions of the gate metals. However, effect of polarization induced charge and trapping effect have not been incorporated and investigated in this work. Chiang *et al.* [13] have presented an analytical subthreshold behavior model of 2D potential, threshold voltage and subthreshold current for short channel tri material gate stack SOI MOSFET based on the exact solution of 2D Poisson's equation. Dhanaselvam *et al.* [14] have performed analytical modeling of triple material surrounding gate (TMSG) MOSFET to obtain surface potential, electric field and threshold voltage by solving 2D Poisson's equation using parabolic approximation method. The advantage of incorporating both TMGS MOSFET and tunnel FET structures in a single device namely triple material surrounding gate tunnel field effect transistor (TMSGTFET) have been proposed by Vanitha *et al.* [17]. An analytical model has been developed based on solution of 2D Poisson's equation in cylindrical coordinate system using parabolic approximation technique. Li *et al.* [18] have performed simulation study of tri material gate FinFET using a 3D device simulator to explore surface potential, electric field and carrier velocity distribution. In all the TMG structures for various FETs, improvements are achieved compared to their corresponding DMG and SMG architectures in terms of (1) suppression of SCEs due to the formation of more steps in surface potential profile and thus screening the impact of drain potential variations and (2) enhancement of carrier transport efficiency as small voltage difference arising from different gate materials leads to uniform electric field distribution along the channel.

1.2 Objectives of the Work

This research is focused on utilizing gate material engineering technique in the form of using three materials with different work functions in the gate electrode of AlGaN/GaN HEMT in order to reduce various short channel effects arising from continuous downscaling of the devices. To the best of our knowledge, no model of this structure has been reported yet. Therefore, the purpose of the proposed work is to develop an analytical model of the device structure to investigate the device physics and characteristics and also to develop its thermal model to study the self-heating effect.

In this work, a two dimensional analytical model of channel potential, electric field and threshold voltage of triple material gate AlGaN/GaN HEMT will be developed. Channel potential of the device will be obtained by solving two dimensional Poisson's equation using proper boundary conditions. Polarization effect and effect of temperature and mole fraction on different device parameters will be taken into consideration to properly perform the formulation and describe the device characteristics. Effect of various trapped charges, formed from defects during the device growth, will be analyzed for more realistic modeling of the device. Several short channel effects like drain induce barrier lowering (DIBL), hot carrier effect, threshold voltage roll off etc. will be explored. Impact of various device parameters such as total channel length, individual metal gate length ratio, AlGaN layer thickness etc. on the device performance will be investigated. A comparative study with other HEMT structures in terms of various device characteristics will be carried out. The proposed model results will be validated against the data obtained from a commercially available numerical device simulator. Finally a simulation model will be developed to investigate the self-heating effect in the device supported on silicon carbide (SiC) substrate and impact of different device parameters and bias voltages on channel temperature will be explored.

1.3 Thesis Outline

The thesis is organized as follows-

Chapter one introduces the topic of the thesis. The motivation behind this thesis work is described in this chapter. This chapter also presents review of related previous researches and shows how other groups have investigated the critical problems associated with AlGaN/GaN HEMTs and made attempts to tackle those. A summary of the definite objectives of the work are also included.

Chapter two presents theoretical background on AlGaN/GaN HEMT. First, structural and electrical properties of GaN are described. Then device structure and polarization effect of AlGaN/GaN HEMT followed by principle of formation of two dimensional electron gas (2DEG) are explained. Finally, second chapter concludes with the description of trapping effect, thermal issues and various applications of AlGaN/GaN HEMT.

Chapter three deals with the device structure and development of the analytical model of channel potential, electric field and threshold voltage of TMG AlGaN/GaN HEMT. Two

dimensional Poisson's equation has been solved using proper boundary conditions to derive the mathematical expression of various device parameters.

Chapter four contains a simulation framework built up to explain self-heating phenomenon in AlGaN/GaN HEMT using finite element method (FEM). The chapter describes the working principles of the simulation model.

Chapter five is devoted to the graphical representation and analysis of the results obtained from the proposed analytical model and authentication of those results with the outcomes found from commercially available 2D device simulator. This chapter shows substantial improvements found in TMG HEMT in terms of reduction of SCEs and enhancement in carrier transport efficiency compared to the other structures.

Chapter six summarizes the overall research work and suggests the scope of future work.

CHAPTER TWO

THEORETICAL BACKGROUND

2.1 Material Properties of Gallium Nitride (GaN):

2.1.1 Structural Properties:

Three types of crystal structures exist for majority of group III-nitride devices: Wurtzite (hexagonal), zinc-blende and rock salt structures. Thermodynamically stable phase under ambient conditions is the Wurtzite structure whereas a metastable type of structure is zinc-blende which is formed when a film is grown on a cubic substrate like GaAs and 3C-SiC. The rock salt structure does not exist naturally and can only be developed under high pressure condition. The Wurtzite structure has a hexagonal unit cell with two lattice constants, a and c as shown in the figure 2.1.

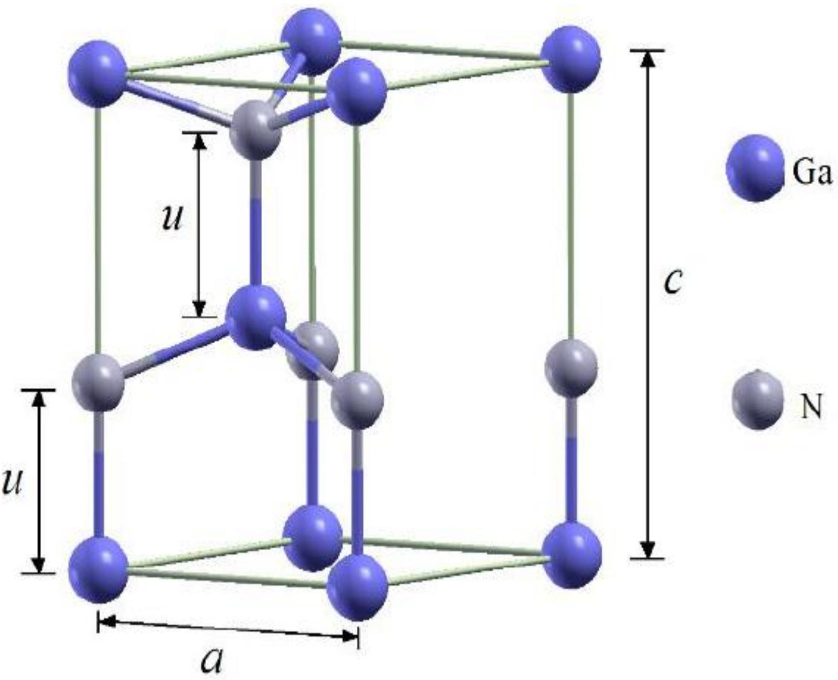

Fig. 2.1 The Wurtzite structure of GaN (Figure is adopted from Ref. [40])

On the other hand, zinc-blende structure has a cubic unit cell and possesses higher degree of crystallographic symmetry because of having equal lattice constants in three perpendicular directions. GaN devices usually exist in Wurtzite structure which can be grown with two

polarities (Ga-face and N-face) along the c axis subject to the atomic order through growth direction [41]. Presence of strong spontaneous and piezoelectric polarization effects is a unique feature of Wurtzite group III-nitride structures [42,43]. Three defining parameters for Wurtzite crystal are the edge length of the basal hexagon (a_0), the height of the hexagonal lattice cell (c_0), and the cation-anion bond length ratio (u_0) along the [0001] direction. Equilibrium lattice parameter values are indicated by the subscript '0'. The values of c_0/a_0 ratio and u_0 are 1.633 and 0.375 in an ideal Wurtzite crystal [40,42].

2.1.2 Electrical Properties:

A semiconductor material should possess the following properties: large energy band gap, high thermal conductivity, low dielectric constant and large breakdown field for high frequency and high power applications. Large band gap enables withstanding high internal electric field before the occurrence of breakdown and provides enhanced radiation resistance. Thermal conductivity of a material defines the ability to dissipate heat from the device efficiently which leads to reduced device temperature and improved performance. Dielectric constant is a measure of the capacitive loading capacity of a transistor and it also affects the device terminal impedance [44]. The dielectric constant of large band-gap semiconductors is nearly 20% lower than the other conventional semiconductors which allows them to be about 20% larger in area for a given impedance. Increased area leads to higher RF currents and higher RF power thereby. Critical electric field for electronic breakdown refers to the maximum amount of electric field that can be supported by the device before breakdown. Large electric field affords large terminal RF voltage and thus generates high RF power. Significant material properties of GaN in comparison with other semiconductor materials are shown in Table 2.1 [45-47].

Band gap of GaN is quite high (3.42 eV) which ensures enhanced performance at high temperature and high voltage conditions [48.49]. The critical field for GaN is around 300 V/µm meaning that for electrodes on GaN with a spacing of 1µm, then theoretically a bias voltage of just above 300 V could be applied without material breakdown. Higher thermal conductivity has made GaN suitable for high power operation. Larger saturated electron drift velocity of GaN compared to other materials facilitates high saturation current and high frequency application. Faster switching frequencies result from GaN HEMT based circuits, as a result, smaller capacitors and inductors are needed which minimize overall size and cost. GaN based devices have been reported to work beyond 300°C [50]. Consequently, there is little need for

large heat sinks and expensive cooling systems. Higher radiation hardness is found in GaN in comparison with GaAs [51]. As a stiff material, GaN is easy to handle mechanically and it is electrically stable too. Moreover, Ga-face GaN crystal shows robust chemical inertness against strong acids and bases [52].

Table 2.1 Material properties of various semiconductor materials

Property	Si	GaAs	4H-SiC	6H-SiC	GaN
Bandgap (eV)	1.12	1.42	3.27	3.02	3.4
Breakdown electric field (MV/cm)	0.3	0.4	3	3.2	3.3
Relative dielectric constant	11.7	12.9	9.7	9.66	8.9
Thermal conductivity (W/m.K)	150	55	370	490	130
Electron mobility (cm^2/V.s)	1400	8500	900	400	1000
Saturated electron drift velocity ($\times 10^7$ cm/s)	1	1	2	2	2.5
Melting point (K)	1415	1238	2827		2791
Hole mobility (cm^2/Vs)	450	400	120	90	200

2.2 AlGaN/GaN HEMT:

Having evolved as an attractive choice as device for micrometer wave power amplifiers and high temperature applications, at present, AlGaN/GaN HEMT is considered as a backbone of both optical and microwave high power electronic applications. Various exciting and unique features like high breakdown electric field, high cut-off frequencies, large current density and high operating temperature have contributed to the superior performance and efficiency of AlGaN/GaN HEMT over other conventional materials used in semiconductor industries till date [40,53].

2.2.1 Device Structure:

A hetero structure is usually formed by joining two different materials with different bandgaps

HEMT, the structure consists of a thin and strained layer of AlGaN on top of a thick relaxed GaN layer. The heterointerface is formed at the junction of these two layers acting as two dimensional electron gas (2DEG) channel which will be described in the subsequent sub-section. AlGaN and GaN layers are known as barrier and buffer layers respectively. The metal contacts used for source and drain terminals are Ohmic contact whereas Schottky contact is used at the gate end. AlGaN can be moderately doped or undoped or unintentionally doped. GaN layer is left undoped.

2.2.2 Polarization:

Polarization effect, existing as a unique feature in III-nitride based structures like AlGaN/GaN HEMTs, plays a dominant role in the origin of electrons resulting in very high carrier concentration, known as 2DEG at the heterointerface of AlGaN and GaN layers. Two types of polarization phenomena namely, spontaneous and piezoelectric polarization are involved in AlGaN/GaN HEMT which are described separately below.

2.2.2.1 Spontaneous polarization:

The presence of the smallest and most electro negative group V element, Nitrogen, gives rise to a polarization in III-nitride structure without any external electric field or deformation which is known as spontaneous polarization. Electronic configuration of nitrogen ($1s^2\ 2s^2\ 2p^3$) implies that it has empty outer orbitals which results in strong attraction of the electrons shared to form the gallium-nitrogen covalent bond by the Coulomb potential of the nitrogen atomic nucleus. Moreover, the Wurtzite III-nitride structure does not possess inversion symmetry along the [0001] direction, which along with strong ionicity of the covalent gallium-nitrogen bond, gives rise to a strong macroscopic spontaneous polarization along the [0001] direction [40,42-43]. The direction of spontaneous polarization vector differs with the polarity of the crystal, whether it is Ga faced or N faced. Spontaneous polarization exists in both GaN and AlGaN layers in AlGaN/GaN HEMT.

2.2.2.2 Piezoelectric polarization:

Mechanical strain induced polarization is known as piezoelectric polarization. Group III-nitride devices show strong piezoelectric polarization effect compared to other III-V structures [54].

A strain causes a perturbation in the bond symmetry of the tetrahedral arrangement of constituent materials as shown in Fig. 2.2.

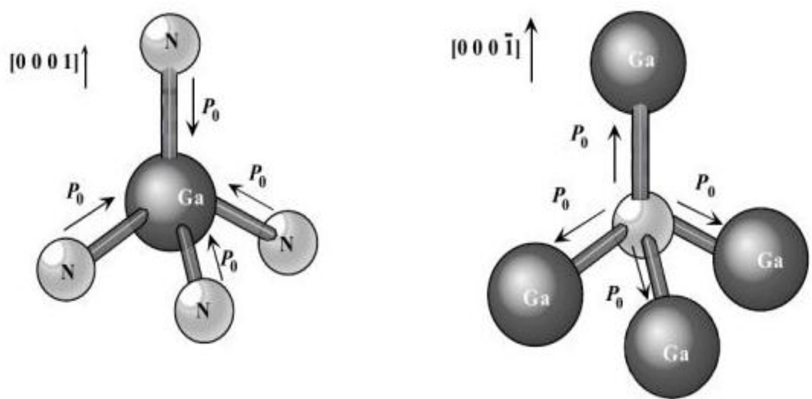

Fig. 2.2 Stick and Ball representation of the tetrahedral arrangement of Ga and N (Figure is adopted from Ref. [54])

Either compressive or tensile strain in the (0001) plane changes the bond angles of atoms at the base vertices and thus changes their vertical components which results in dipole moment along the [0001] direction. In AlGaN/GaN HEMT, piezoelectric polarization occurs in AlGaN layer from tensile strain induced by the stress because of the lattice constant mismatch between AlGaN and GaN. Because of comparatively large thickness, GaN layer is fully relaxed and does not suffer from any stress. As a result, no piezoelectric polarization exist in GaN.

Two types of polarizations and their directions are shown in Fig. 2.3 where P_{SP} represents spontaneous polarization while P_{PE} indicates piezoelectric polarization.

When AlGaN layer is grown on top of GaN layer, their difference in polarization causes a net polarization charge developed at the interface depending on the growth face of the crystal. In Ga faced GaN and AlGaN layers grown on c axis, polarization induced net charge bound at the interface is positive [20] as shown in Fig 2.3. Although a positive charge develops at the bottom of GaN resulting from the polarization, a negligible effect of such charge on 2DEG is encountered because of the presence of large number of electrons, traps and defects between 2DEG and GaN layer which cancel those charges and thus, the effect of this charge is ignored in all computations [44]. Spontaneous and piezoelectric induced charges will be opposite if the face of growth of the crystal is changed from Ga to N.

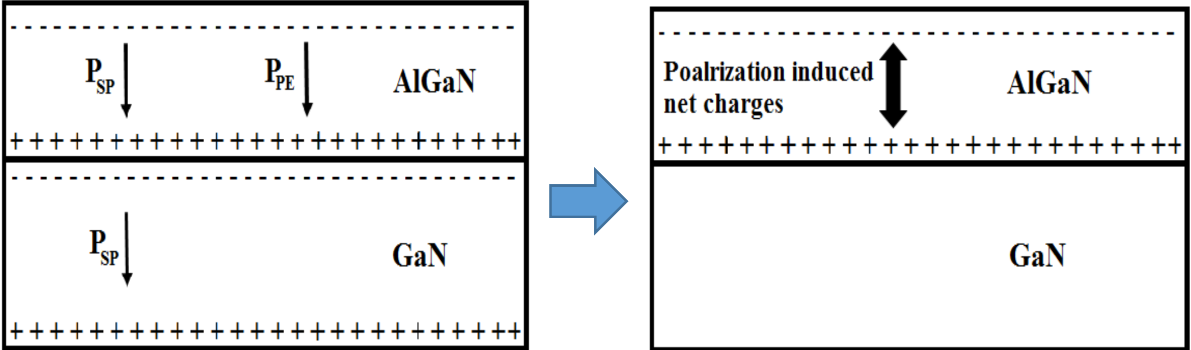

Fig. 2.3 Spontaneous and piezoelectric polarization field induced charges in AlGaN/GaN HEMT

2.2.3 Formation of Two Dimensional Electron Gas (2DEG):

The conduction band energy band diagram for the AlGaN/GaN HEMT is shown in Fig. 2.4.

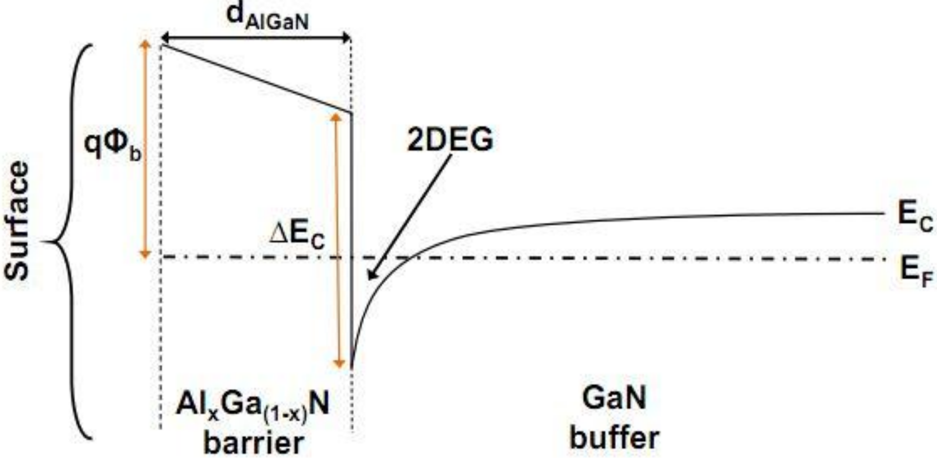

Fig. 2.4 Conduction band energy band diagram of AlGaN/GaN heterostructure (adopted from [56])

The wider band gap AlGaN is shown to the left side and the comparatively narrower band gap GaN on the right. The difference in conduction band energies at the interface of the materials results in a conduction band offset ΔE_C and a triangular quantum well is formed where the electrons which make up the 2DEG will tend to due to preferable (lower) energy. The origin and cause of the accumulation of electrons at the heterointerface leading to formation of 2DEG is described below.

To compensate the polarization induced positive sheet charge density at the interface of the AlGaN/GaN HEMT, electrons accumulate at the interface and confine in the GaN layer adjacent to the heterointerface to build up a 2DEG because of the presence of the triangular quantum well. Many researches have been performed in the last few years to investigate the source of electrons for formation of 2DEG [29,42-43,57-59]. There are three types of charges present in the structure : polarization induced charge at the heterointerface and the AlGaN surface ($\pm\sigma_{pol}$), charge because of electrons in 2DEG channel (n_{2DEG}) and charge at AlGaN surface formed by states due to broken bonds and other surface defects ($\pm\sigma_s$). Another source of charge arises from doping in the AlGaN layer. But this charge needs not to be taken into account if the barrier layer is left undoped. The polarization induced sheet charge is balanced, so charge neutrality equation implies that

$$\sigma_s - n_{2DEG} = 0$$

So surface states acts as the source of electrons in 2DEG [60]. The position of the energy level of these surface states with respect to the Fermi level determines the availability of electrons for accumulation in 2DEG channel depending on the thickness of the barrier layer [58,60]. Initially, with no electrons in 2DEG, there exists an electric field due to polarization induced charges present at both sides of AlGaN layer. Surface donor states exist at a particular energy level in the forbidden gap measured relative to the conduction band minimum of the AlGaN surface. With increasing barrier thickness t, this level moves higher due to the constant electric field in the barrier. Once this level reaches the Fermi level, the surface donor states start donating electrons to form the 2DEG at the AlGaN/GaN interface and positive surface sheet charge is left behind [55]. The dipole strength reduces with the increase of electrons in 2DEG channel which gradually reduces the electric field and causes saturated 2DEG density after a critical thickness of the barrier layer [58]. If the barrier layer is doped (n type), additional source of electron in 2DEG channel comes from donor impurities. These electrons diffuse across the heterointerface to GaN and become confined at the quantum well to add to the 2DEG. Thus the total 2DEG concentration depends on polarization effects, doping concentration in the barrier layer and conduction band offset.

2.2.4 Trapping Effect:

Trap states present in AlGaN/GaN HEMT can limit the output power performance and efficiency to a large extent. The term trap refers to the energy states in the band gap of the semiconductor arising from crystal defects, dislocation and impurities. Till now, various trapping effects have been explored including current collapse of drain characteristics, gate and drain lag transients, light sensitivity, transconductance frequency dispersion and limited microwave output power [29]. Locations of trapped charge include AlGaN surface, AlGaN/GaN hetero interface and GaN buffer layer as shown in Fig. 2.5.

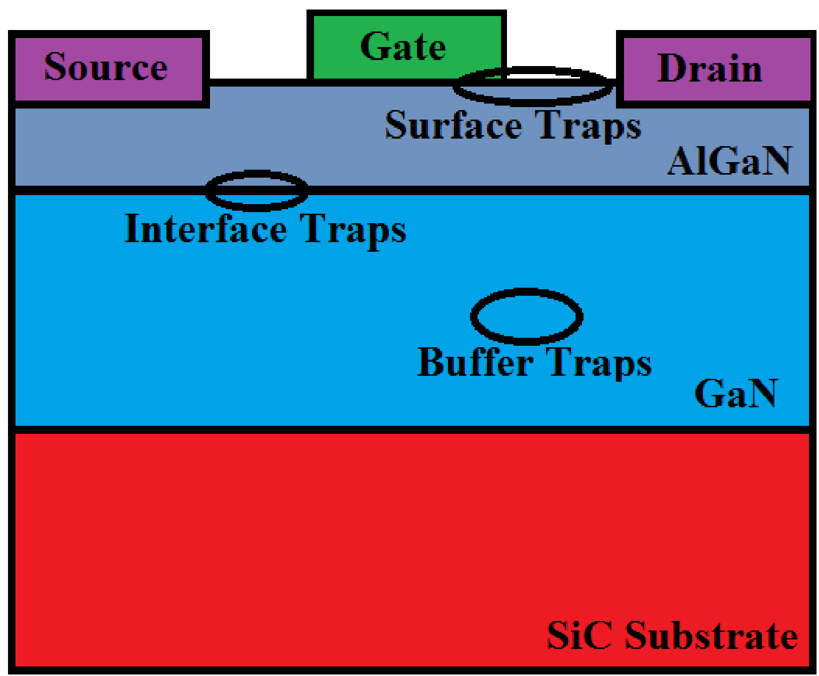

Fig. 2.5 Possible location of trap states in AlGaN/GaN HEMT

Surface traps: The atomic layer at the surface has unterminated or dangling bonds resulting from perturbation of the perfect periodicity of the crystal lattice. Therefore band structure can be changed at the surface and localized energy states can exist in the forbidden energy band gap. Two types of surface trap states - intrinsic surface states and defect associated extrinsic surface states can occur in the structure. Intrinsic surface states exist in an ideally perfect surface and correspond to solution of Schrodinger equation with energy levels within the forbidden band gap. Defects and impurities at the surface result in developing extrinsic surface states which are formed during crystal growth or in subsequent device fabrication process. These surface states act as donor traps [61] and are major source of electrons in forming 2DEG,

as discussed in the previous subsection. Change in the density of surface traps provokes a noteworthy change in 2DEG density. Such traps are also responsible for current collapse and gate tunneling phenomena [62-63].

Interface traps: Interface traps are formed because of interruption of the periodicity of the crystal lattice at the heterointerface. The lattice constant mismatch and inherent stress in the material interfaces form point defects and threading dislocations in the material which appear as defect levels inside the energy band gap. Some additional defect levels in the band gap are also created by unintended impurities present in the material during device fabrication process. Based on trap type, these defect energy levels can capture electrons or holes and trap them for a long time because of their closeness to conduction band minimum or valence band maximum [61]. Consequently, 2DEG density in the channel decreases which results in reduction in output current.

Buffer traps: Imperfectly grown crystal with impurities, defects and dislocations in the GaN material leads to the formation of deep level trap states within GaN layer which are known as buffer traps. Mobile electrons in the 2DEG channel may get injected into the buffer traps because of high drain-source voltage applied. The trapped electrons cannot follow the high frequency signal owing to the large trapping time constant of the order of milliseconds [62]. These trapped electrons generate negative charge, deplete the 2DEG and abate the channel current. However, as these trap states lie deep below the conduction band edge and have large time constants, their effects may be disregarded.

2.2.5 Thermal Properties:

High electron concentration and current flow offered in GaN based transistors produce heat across the device by Joule heating effect which is known as self-heating. This heating phenomenon takes place during the interaction of conduction electrons and atoms of the semiconductor. Phonon, quantized energy package, is generated by the vibration of the crystal lattice. When collisions occur between the electrons and the atoms of the crystal during the flow of electrons inside the device, energy is transmitted to the lattice from the highly energetic electrons and hot phonons are launched. These phonons remain localized in the regions of electron flow, accrue and store energy, which ultimately releases as heat. Self-heating poses a severe problem for the device by degrading its electrical performance [64]. Channel

temperature can rise to a huge amount above the ambient temperature because of this self-heating effect. This increase in temperature results in modification of the temperature dependent parameters like bandgap, threshold voltage, sheet carrier concentration, mobility etc. Mobility reduction with temperature increase causes decrease in current and maximum power density and increase in gate leakage current. Substrate on which the device is supported plays a significant role in determining the amount of self-heating. Usually, sapphire (Al_2O_3), Silicon Carbide (SiC), silicon (Si) are used as substrate materials for GaN based HEMTs. Issues regarding the materials used as substrate are described below:

1) Sapphire : High melting point and availability have made sapphire (Al_2O_3) a familiar material for using as substrate. The main disadvantage of this material is low thermal conductivity (42 $Wm^{-1}K^{-1}$) [65] which may cause overheating the device.

2) Silicon : Intrinsic silicon is a popular substrate material for GaN HEMTS. But a nucleation layer is to be introduced due to lattice mismatch which increases distance between the channel and substrate [66].

3) Silicon Carbide : High thermal conductivity has made Silicon Carbide a standard choice for substrate material in high power GaN HEMTs. But defects present in SiC makes growth of GaN layer difficult because of the occurrence of non-uniformity during the crystal growth procedure. [65].

4) Bulk GaN : Bulk GaN substrate can support high temperature operation but by itself it cannot sufficiently remove the generated heat during device operation.

Table 2.2 Thermal conductivities of familiar substrate materials

Substrate	Thermal conductivity (W/m.K)
Sapphire	42
Silicon	150
Silicon carbide	490
GaN	130

Table 2.2 shows thermal conductivity values of different substrate materials.

2.2.6 Applications :

Major fields of applications of GaN based electronics include high efficiency and high linearity power amplifiers for base stations in 4G wireless broadband cellular networks, hybrid electric vehicles platform, high-voltage power rectifiers (inverter modules), switches (plasma display panels, low-frequency high-power switching), high-frequency MMICs (wireless broadband communication links), high temperature electronics (automotive, energy production), micro electro-mechanical systems, military and commercial aircraft engine electronics, MEMS (pressure sensors) and Hall sensors (automotive applications). [40,42,53] AlGaN/GaN HEMT is also used for construction of high temperature digital integrated circuits (IC) which can be utilized in chemical reactors, aviation system, intelligent control and sensing circuits for automotive engines. AlGaN/GaN HEMTs can work with less cooling and inexpensive processing steps for maximizing heat extraction. Moreover, AlGaN/GaN HEMTs exhibit on resistance value of $<1 m\Omega cm^2$ compared to $>100 m\Omega cm^2$ for Si which results in reduced on-state power loss and improved performance.

CHAPTER THREE

ANALYTICAL MODELING OF PROPOSED DEVICE

3.1 Device Structure:

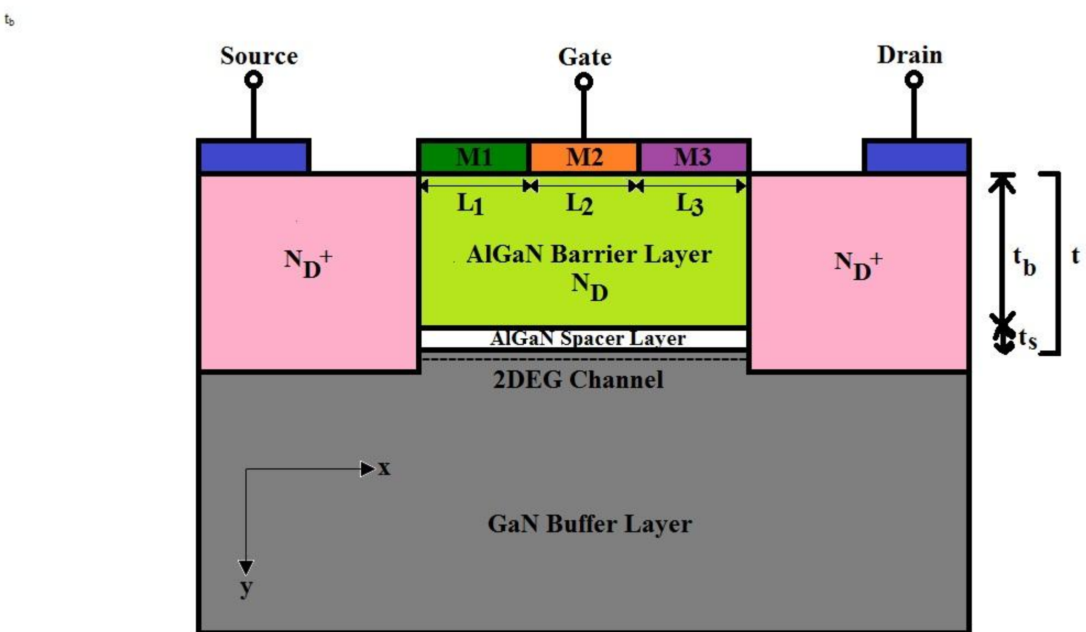

Fig. 3.1 Two dimensional schematic diagram of Triple Material Gate $Al_{0.3}Ga_{0.7}N$/GaN HEMT

Fig. 3.1 shows the schematic structure of TMG HEMT used in our work. The device consists of an n-doped barrier layer of wider bandgap material AlGaN, an undoped spacer layer of AlGaN and a buffer layer of narrow bandgap material, GaN. The spacer layer is introduced to increase the distance between ionized donor atoms and electron gas formed in the 2DEG channel and thus probability of impurity scattering is further diminished. M1, M2 and M3 are three laterally connected gate contact forming metals with distinct work functions of Φ_{M1}, Φ_{M2} and Φ_{M3} respectively and L_1, L_2 and L_3 are their corresponding lengths. Metal with Φ_{M1} possesses the largest work function among the three which is placed near the source end and the metal having Φ_{M3}, which is placed near the drain contact contains the smallest work function with respect to the other gate metals. Total AlGaN layer thickness, $t = t_b+t_s$, where t_b is the barrier layer and t_s is the spacer layer thicknesses respectively. Gate and drain bias voltages are denoted as V_{gs} and V_{ds} and are assumed to be -0.2V and 0.2V respectively unless stated otherwise and the source is kept grounded.

3.2 Channel Potential:

This section presents the modeling of two dimensional (2D) potential distribution of a triple material gate HEMT. Assuming uniform doping density in the channel area and fully depleted region under the gate at normal working conditions which is due to the combined effect of Schottky barrier at the surface and diffusion of electron into the channel at the heterojunction, we solve 2D Poisson's equation to obtain two dimensional electrostatic potential, $\Phi(x, y)$ as

$$\frac{\partial^2\Phi(x,y)}{\partial x^2}+\frac{\partial^2\Phi(x,y)}{\partial y^2}=\frac{-qN_D}{\varepsilon_s} \qquad 0\le x\le L \tag{1}$$

where q is the electron charge, N_D is the impurity density of AlGaN barrier layer, ε_s is the permittivity of $Al_mGa_{1-m}N$ and can be expressed as a function of mole fraction of Al [6]

$$\varepsilon_s = 9.5 - 0.5m \tag{2}$$

where m is Al mole fraction in AlGaN.

The solution of Eq (1) i.e. the potential distribution along the vertical direction can be approximated by a second order polynomial function as

$$\Phi(x,y)=a_0(x)+a_1(x)(y-t)+a_2(x)(y-t)^2 \tag{3}$$

Here, $a_0(x)=\Phi_c(x)$ is the potential at the hetero interface location and called channel potential, a_1 and a_2 are arbitrary constants.

As the gate terminal is composed of three different materials placed side by side, the potential distribution under three metal regions (M1, M2 and M3) is given by

$$\Phi_i(x,y)=\Phi_{ci}(x)+a_{i1}(x)(y-t)+a_{i2}(x)(y-t)^2 \tag{4}$$

the symbol i represents three separate regions under three metal gates with different work functions which is defined as

$$i=\begin{cases}1, & 0\le x\le L_1\\ 2, & L_1\le x\le L_1+L_2\\ 3, & L_1+L_2\le x\le L_1+L_2+L_3\end{cases} \tag{5}$$

Parameters in Eq. (4) for three different values of i can be obtained by applying the following boundary conditions,

1. The potential at the AlGaN surface after applying the gate to source voltage, V_{gs} is found as,

$$\Phi_i(x,0) = V_{gsi} \tag{6}$$

where

$$V_{gsi} = V_{gs} - V_{FBi} \tag{7}$$

V_{FBi} are flat band voltages of the three metal gates which can be found from the following relationships,

$V_{FB1} = \Phi_{M1} - \Phi_a$, $V_{FB2} = \Phi_{M2} - \Phi_a$ and $V_{FB3} = \Phi_{M3} - \Phi_a$.

Φ_a is the work function of AlGaN and is given by,

$$\Phi_a = \chi_a + \frac{E_{g,AlGaN}}{2} - \Phi_f \tag{8}$$

where χ_a is the electron affinity of AlGaN, $E_{g,AlGaN}$ is the energy bandgap of AlGaN at T = 300K and Φ_f is the Fermi potential which is expressed as

$$\Phi_f = V_T \ln\left(\frac{N_D}{N_i}\right) \tag{9}$$

where $V_T = \frac{k_B T}{q}$ is the thermal voltage at T = 300K, k_B is the Boltzmann constant and N_i is the intrinsic carrier concentration.

2. Channel potentials at the interfaces of the metal gate 1 and 2 and metal gate 2 and 3 are continuous.

$$\Phi_1(L_1, t) = \Phi_2(L_1, t) \tag{10}$$

$$\Phi_2(L_1 + L_2, t) = \Phi_3(L_1 + L_2, t) \tag{11}$$

3. Electric fields at the interfaces of the metal gate 1 - 2 and metal gate 2 - 3 are continuous.

$$\left.\frac{d\Phi_1(x,y)}{dx}\right|_{x=L_1} = \left.\frac{d\Phi_2(x,y)}{dx}\right|_{x=L_1} \tag{12}$$

$$\left.\frac{d\Phi_2(x,y)}{dx}\right|_{x=L_1+L_2} = \left.\frac{d\Phi_3(x,y)}{dx}\right|_{x=L_1+L_2} \tag{13}$$

4. Electric fields at the heterointerface for three different metal gates are given by,

$$\left.\frac{d\Phi_i(x,y)}{dy}\right|_{y=t} = -E_{he,i} \tag{14}$$

where $E_{he,i}$ is given in [67] as

$$E_{he,i} = \frac{qN_{si}}{\varepsilon_s} \tag{15}$$

where N_{si} is the sheet carrier concentration in the 2DEG channel and is given in [68] by

$$N_{si} = \frac{-p_2 + \sqrt{p_2^{\,2} + 4p_4(V_{gsi} - V_{ai})}}{2p_4} \tag{16}$$

where p_1, p_2, p_3 and p_4 are temperature dependent parameters and are expressed as follows

$$p_1 = b_1T^3 + b_2T^2 + b_3T + b_4 \tag{17}$$

$$p_2 = k_1T^5 + k_2T^4 + k_3T^3 + k_4T^2 + k_5T + k_6 \tag{18}$$

$$p_3 = h_1T^3 + h_2T^2 + h_3T + h_4 \tag{19}$$

$$p_4 = p_3 + \frac{qt}{\varepsilon_s} \tag{20}$$

The arbitrary constants, b_1-b_4, k_1-k_6 and h_1-h_4 in Eq. (17) – (19) can be found from [69]

V_{ai} in Eq. (16) is defined as

$$V_{ai} = V_{oi} + p_1 \tag{21}$$

Where V_{oi} is the voltage required to annihilate the 2DEG and is given in [69] as

$$V_{oi} = \frac{\Phi_{sbi}}{q} - \frac{\Delta E_c}{q} - \frac{qN_Dt_b^{\,2}}{2\varepsilon_s} - \frac{t\sigma_{pol}}{\varepsilon_s} - \frac{qtN_{tr}}{\varepsilon_s} \tag{22}$$

Here, Φ_{sbi} is the Schottky barrier height for three different gate metals, N_{tr} is the net charged traps per unit area, ΔE_c is the conduction band offset at the AlGaN/GaN interface and is given in [6] as

$$\Delta E_c = 0.7(E_{g,Al_mGa_{1-m}N} - E_{g,GaN}) \tag{23}$$

$E_{g,Al_mGa_{1-m}N}$ is bandgap of AlGaN which can be expressed as a function of temperature and mole fraction like below [69]

$$E_{g,Al_mGa_{1-m}N}(m,T) = E_{g,Al_mGa_{1-m}N,RT}(m) + \Delta E_g - \frac{2\delta_{GaN}}{\exp(\frac{\tau_{GaN}}{T} - 1)} \tag{24}$$

where δ_{GaN} is the electron-phonon coupling constant, τ_{GaN} is the average phonon temperature, $E_{g,Al_mGa_{1-m}N,RT}(m)$ is the bandgap of AlGaN at room temperature which is a function of Al mole fraction and is given by [69],

$$E_{g,Al_mGa_{1-m}N,RT}(m) = 6.13m + 3.42(1-m) - m(1-m) \tag{25}$$

Energy bandgap of GaN, $E_{g,GaN}$ is expressed as in [69],

$$E_{g,GaN}(T) = E_{g,GaN}(0) - \frac{2\delta_{GaN}}{\exp(\frac{\tau_{GaN}}{T} - 1)} \tag{26}$$

σ_{pol} in Eq. (22) is the polarization induced sheet charge density at the 2DEG channel and is given by [6]

$$|\sigma_{pol}| = |P_{piezo}(Al_mGa_{1-m}N) + P_{spon}(Al_mGa_{1-m}N) - P_{spon}(GaN)| \tag{27}$$

$P_{piezo}(Al_mGa_{1-m}N)$ is the sheet carrier density induced by piezoelectric polarization of AlGaN and is given by [6]

$$P_{piezo}(Al_mGa_{1-m}N) = \frac{2[d(0) - d(m)]}{d(m)}[e_{31}(m) - \frac{e_{33}(m)C_{13}(m)}{C_{33}(m)}] \tag{28}$$

where d is the lattice constant parameter, C_{13}, C_{33} are the elastic constant parameters and e_{31}, e_{33} are piezoelectric constants which are expressed as follows [6]

$$d(m) = (0.3189 - 0.0077m) \text{ nm} \tag{29}$$

$$C_{13}(m) = (103 + 5m)\ \text{GPa} \tag{30}$$

$$C_{33}(m) = (405 - 32m)\ \text{GPa} \tag{31}$$

$$e_{31}(m) = (-0.49 - 0.11m)\ \text{C/m}^2 \tag{32}$$

$$e_{33}(m) = (0.73 + 0.73m)\ \text{C/m}^2 \tag{33}$$

For AlGaN layer, spontaneous polarization induced sheet charge density, $P_{spon}\left(Al_mGa_{1-m}N\right)$ is given by,

$$P_{spon}\left(Al_mGa_{1-m}N\right) = (-0.029 - 0.052m)\ \text{C/m}^2 \tag{34}$$

For GaN layer, the sheet carrier density due to spontaneous polarization, $P_{spon}\left(GaN\right)$ is -0.029 C/m^2

5. The potential at the source-channel interface is

$$\Phi_1(0,t) = \Phi_{bi} = \Phi_{c1}(0) \tag{35}$$

where Φ_{bi} is the built in potential [70].

6. The potential at the drain-channel interface is given by

$$\Phi_1(L_1 + L_2 + L_3, t) = \Phi_{bi} + V_{ds} = \Phi_{c1}(L_1 + L_2 + L_3) \tag{36}$$

Taking derivative of Eq. (4) with respect to y at the heterointerface and using Eq. (14), we get

$$a_{i1}(x) = -E_{he,i} \tag{37}$$

Using Eq. (37), we get from Eq. (4) and (6)

$$a_{i2}(x) = \frac{V_{gsi} - \Phi_{ci}(x) - tE_{he,i}}{t^2} \tag{38}$$

Eq. (4) can be expressed as using Eq. (37) and (38)

$$\Phi_i(x,y) = \Phi_{ci}(x) - E_{he,i}(y-t) + \left[\frac{V_{gsi} - \Phi_{ci}(x) - tE_{he,i}}{t^2}\right](y-t)^2 \tag{39}$$

With the help of Eq. (39), Eq. (1) can now be represented as

$$\frac{\partial^2\Phi_{ci}(x)}{\partial x^2}+\frac{V_{gsi}-\Phi_{ci}(x)}{\alpha^2}=-\frac{qN_D}{\varepsilon_s}+\frac{2E_{he,i}}{t} \tag{40}$$

where α is given by

$$\alpha=\frac{t}{\sqrt{2}} \tag{41}$$

Eq. (40) can be represented in a reduced form as follows

$$\frac{\partial^2\beta_i(x)}{\partial x^2}-\frac{\beta_i(x)}{\alpha^2}=0 \tag{42}$$

by taking $$\beta_i(x)=\Phi_{ci}(x)-V_{gsi}-\left(\frac{qN_D}{\varepsilon_s}-\frac{2E_{he,i}}{t}\right)\alpha^2 \tag{43}$$

General solution to Eq. (42) can be written as

$$\beta_i(x)=A_ie^{\Psi x}+B_ie^{-\Psi x}\ \text{ where }\ \Psi=\frac{1}{\alpha} \tag{44}$$

The coefficients A_i and B_i in Eq. (44) can be found by using the previously stated boundary conditions and solving the corresponding equations,

$$A_1=\frac{1}{2\sinh(\Psi L)}\{(\Phi_{bi}+V_{ds}-V_{gs3}-c_3\alpha^2)-e^{-\Psi L}(\Phi_{bi}-V_{gs1}-c_1\alpha^2)+[(V_{gs2}-V_{gs1})+(c_2-c_1)\alpha^2]$$
$$\cosh[\Psi(L_2+L_3)]+[(V_{gs3}-V_{gs2})+(c_3-c_2)\alpha^2]\cosh(\Psi L_3)\} \tag{45}$$

$$A_2=A_1-\frac{1}{2}e^{-\Psi L_1}[(V_{gs2}-V_{gs1})+(c_2-c_1)\alpha^2] \tag{46}$$

$$A_3=A_1-\frac{1}{2}e^{-\Psi L_1}[(V_{gs2}-V_{gs1})+(c_2-c_1)\alpha^2]-\frac{1}{2}e^{-\Psi(L_1+L_2)}[(V_{gs3}-V_{gs2})+(c_3-c_2)\alpha^2] \tag{47}$$

$$B_1=(\Phi_{bi}-V_{gs1}-c_1\alpha^2)-A_1 \tag{48}$$

$$B_2=B_1-\frac{1}{2}e^{\Psi L_1}[(V_{gs2}-V_{gs1})+(c_2-c_1)\alpha^2] \tag{49}$$

$$B_3 = B_1 - \frac{1}{2}e^{\Psi L_1}[(V_{gs2} - V_{gs1}) + (c_2 - c_1)\alpha^2] - \frac{1}{2}e^{\Psi(L_1+L_2)}[(V_{gs3} - V_{gs2}) + (c_3 - c_2)\alpha^2] \quad (50)$$

where $$c_i = \frac{qN_D}{\varepsilon_s} - \frac{2E_{he,i}}{t} \quad (51)$$

Putting the corresponding A_i and B_i values in Eq. (44), solving for $\beta_i(x)$ and then from (43), expression for the channel potential, Φ_{ci} under three different metal gate regions (i = 1,2,3) can be presented as

$$\Phi_{ci}(x) = A_i e^{\Psi x} + B_i e^{-\Psi x} + V_{gsi} + c_i\alpha^2 \quad (52)$$

3.3 Electric Field:

The electric field along the channel is an important parameter as it determines the carrier transport velocity. The electric field profile under the three metal gate regions along the channel is found by taking derivative of potential functions expressed in Eq. (39) with respect to x at the hetero interface location (y =t) and is given by

$$E_1(x) = \left.\frac{d\Phi_1(x,y)}{dx}\right|_{y=t} \quad (53)$$

$$= \frac{d\Phi_{c1}(x)}{dx}$$

$$= \frac{1}{\sinh(\Psi L)}\{\Psi([(\Phi_{bi} + V_{ds}) - V_{gs3} - c_3\alpha^2] + [(V_{gs2} - V_{gs1}) + (c_2 - c_1)\alpha^2]$$

$$\cosh[\Psi(L_2 + L_3)] + [(V_{gs3} - V_{gs2}) + (c_3 - c_2)\alpha^2]\cosh[\Psi L_3])\cosh[\Psi x] - \Psi(\Phi_{bi} - V_{gs1} - c_1\alpha^2)$$

$$\cosh[\Psi(L - x]\} \quad (54)$$

$$E_2(x) = \left.\frac{d\Phi_2(x,y)}{dx}\right|_{y=t} \quad (55)$$

$$= \frac{d\Phi_{c2}(x)}{dx}$$

$$= \frac{1}{\sinh(\Psi L)}\{\Psi([(\Phi_{bi}+V_{ds})-V_{gs3}-c_3\alpha^2]+[(V_{gs2}-V_{gs1})+(c_2-c_1)\alpha^2]$$

$$\cosh[\Psi(L_2+L_3)]+[(V_{gs3}-V_{gs2})+(c_3-c_2)\alpha^2]\cosh[\Psi L_3])\cosh[\Psi x]-\Psi(\Phi_{bi}-V_{gs1}-c_1\alpha^2)$$

$$\cosh[\Psi(L-x]-\Psi[(V_{gs2}-V_{gs1})+(c_2-c_1)\alpha^2]\sinh[\Psi L]\sinh[\Psi(x-L_1)]\} \quad (56)$$

$$E_3(x)=\left.\frac{d\Phi_3(x,y)}{dx}\right|_{y=t} \quad (57)$$

$$=\frac{d\Phi_{c3}(x)}{dx}$$

$$=$$

$$\frac{1}{2\sinh(\Psi L)}\{2\Psi[(\Phi_{bi}+V_{ds})-V_{gs3}-c_3\alpha^2]\cosh(\Psi x)-2\Psi(\Phi_{bi}-V_{gs1}-c_1\alpha^2)\cosh[\Psi(L-x]$$

$$+[(V_{gs2}-V_{gs1})+(c_2-c_1)\alpha^2][\Psi\cosh[\Psi(x-2L_1-L_2-L_3)]+\Psi\cosh[\Psi(x-L_2-L_3)]]$$

$$+[(V_{gs3}-V_{gs2})+(c_3-c_2)\alpha^2][\Psi\cosh[\Psi(x-2L_1-2L_2-L_3)]+\Psi\cosh[\Psi(x-L_3)]]\} \quad (58)$$

3.4 Minimum Channel Potential:

As three gate metals with different work functions coexist in the TMG HEMT structure, the gate metal with the highest work function determines the minimum channel potential. Therefore, the region under M1 contains the position at which this channel potential minima occurs. Differentiating $\Phi_{c1}(x)$ with respect to x and equating the derivative to zero gives the minimum channel potential location which is given by,

$$x_{min}=\frac{1}{2\Psi}\ln(\frac{B_1}{A_1}) \quad (59)$$

where A_1 and B_1 can be found from Eq. (45) and (48) respectively.

The value of the minimum channel potential is found by replacing the value of x_{min} with i=1 in Eq. (52) and is given by

$$\Phi_{c1,min}(x_{min})=A_1e^{\Psi x_{min}}+B_1e^{-\Psi x_{min}}+V_{gs1}+c_1\alpha^2 \quad (60)$$

So, $$\Phi_{c1,min}(x_{min}) = \frac{1}{\sinh(\Psi L)}\{[(\Phi_{bi}+V_{ds})-V_{gs3}-c_3\alpha^2]\sinh(\Psi x_{min})+(\Phi_{bi}-V_{gs1}-c_1\alpha^2)$$

$$\sinh[\Psi(L-x_{min})]+[(V_{gs2}-V_{gs1})+(c_2-c_1)\alpha^2]\sinh(\Psi x_{min})\cosh[\Psi(L_2+L_3)]$$

$$+[(V_{gs3}-V_{gs2})+(c_3-c_2)\alpha^2]\sinh(\Psi x_{min})\cosh(\Psi L_3)\}+V_{gs1}+c_1\alpha^2 \quad (61)$$

3.5 Threshold Voltage:

Equating the channel potential minima, $\Phi_{c1,min}(x_{min})$ with twice the value of Fermi potential and solving for the corresponding V_{gs} give the threshold voltage, V_{th}. Hence at threshold condition, the following can be deduced from Eq. (59), (60), (51) and (7) for i = 1,

$$2\Phi_f = 2\sqrt{A_{1th}B_{1th}} + V_{th} - V_{FB1} + \left(\frac{qN_D}{\varepsilon_s} - \frac{2E_{he,1th}}{t}\right)\alpha^2 \quad (62)$$

where $A_{1th} = A_1$, $B_{1th} = B_1$ and $E_{he,1th} = E_{he,1}$ at $V_{gs} = V_{th}$

After some manipulation, Eq. (62) takes the form of Eq. (63)

$$DV_{th}^2 + EV_{th} + F = 0 \quad (63)$$

where $$D = X^2 + 4MS \quad (64)$$

$$E = (-2XG) + 4(PS - MR) \quad (65)$$

$$F = G^2 - 4PR \quad (66)$$

$$X = 1 - \frac{2}{t}\frac{q}{\varepsilon_s}\alpha^2\frac{1}{p_4}\left(1-\frac{p_2}{p_{c1}}\right) \quad (67)$$

$$p_{ci}^2 = p_2^2 - 4p_4V_{ai} \quad (68)$$

$$M = \frac{1}{2\sinh(\Psi L)}\{[-1+\frac{2}{t}\alpha^2\frac{q}{\varepsilon_s}\frac{1}{p_4}(1-\frac{p_2}{p_{c3}})]-[-1+\frac{2}{t}\alpha^2\frac{q}{\varepsilon_s}\frac{1}{p_4}(1-\frac{p_2}{p_{c1}})]e^{-\Psi L}+\cosh(\frac{L_2+L_3}{\alpha})$$

$$[\frac{2}{t}\alpha^2\frac{q}{\varepsilon_s}\frac{1}{p_4}(1-\frac{p_2}{p_{c1}})-\frac{2}{t}\alpha^2\frac{q}{\varepsilon_s}\frac{1}{p_4}(1-\frac{p_2}{p_{c2}})]+\cosh(\frac{L_3}{\alpha})[\frac{2}{t}\alpha^2\frac{q}{\varepsilon_s}\frac{1}{p_4}(1-\frac{p_2}{p_{c2}})$$

$$-\frac{2}{t}\alpha^2\frac{q}{\varepsilon_s}\frac{1}{p_4}(1-\frac{p_2}{p_{c3}})]\} \tag{69}$$

$$S=1-\frac{2}{t}\alpha^2\frac{q}{\varepsilon_s}\frac{1}{p_4}(1-\frac{p_2}{p_{c1}})+M \tag{70}$$

$$G=V_{FB1}+2\Phi_f-\frac{qN_D}{\varepsilon_s}\alpha^2+\frac{2}{t}\alpha^2\frac{q}{\varepsilon_s}\frac{1}{4p_4{}^2}(p_2-p_{c1})^2-\frac{2}{t}\alpha^2\frac{q}{\varepsilon_s}\frac{1}{p_4}V_{FB1}(1-\frac{p_2}{p_{c1}}) \tag{71}$$

$$P=\frac{1}{2\sinh(\Psi L)}\{[(\Phi_{bi}+V_{ds}+V_{FB3}-\frac{qN_D}{\varepsilon_s}\alpha^2+\frac{2}{t}\alpha^2\frac{q}{\varepsilon_s}\frac{1}{4p_4{}^2}(p_2-p_{c3})^2-\frac{2}{t}\alpha^2\frac{q}{\varepsilon_s}\frac{V_{FB3}}{p_4}(1-\frac{p_2}{p_{c3}})]$$

$$-[\Phi_{bi}+V_{FB1}-\frac{qN_D}{\varepsilon_s}\alpha^2+\frac{2}{t}\alpha^2\frac{q}{\varepsilon_s}\frac{1}{4p_4{}^2}(p_2-p_{c1})^2-\frac{2}{t}\alpha^2\frac{q}{\varepsilon_s}\frac{V_{FB1}}{p_4}(1-\frac{p_2}{p_{c1}})]\,e^{-\Psi L}$$

$$+[\cosh(\frac{L_2+L_3}{\alpha})(V_{FB1}-V_{FB2})+\cosh(\frac{L_2+L_3}{\alpha})[\frac{2}{t}\alpha^2\frac{q}{\varepsilon_s}\frac{1}{4p_4{}^2}(p_2-p_{c1})^2-\frac{2}{t}\alpha^2\frac{q}{\varepsilon_s}\frac{V_{FB1}}{p_4}(1-\frac{p_2}{p_{c1}})$$

$$-\frac{2}{t}\alpha^2\frac{q}{\varepsilon_s}\frac{1}{4p_4{}^2}(p_2-p_{c2})^2+\frac{2}{t}\alpha^2\frac{q}{\varepsilon_s}\frac{V_{FB2}}{p_4}(1-\frac{p_2}{p_{c2}})]+\cosh(\frac{L_3}{\alpha})[(V_{FB2}-V_{FB3})$$

$$+\frac{2}{t}\alpha^2\frac{q}{\varepsilon_s}\frac{1}{4p_4{}^2}(p_2-p_{c2})^2-\frac{2}{t}\alpha^2\frac{q}{\varepsilon_s}\frac{V_{FB2}}{p_4}(1-\frac{p_2}{p_{c2}})-\frac{2}{t}\alpha^2\frac{q}{\varepsilon_s}\frac{1}{4p_4{}^2}(p_2-p_{c3})^2$$

$$+\frac{2}{t}\alpha^2\frac{q}{\varepsilon_s}\frac{V_{FB3}}{p_4}(1-\frac{p_2}{p_{c3}})]\} \tag{72}$$

$$R=\Phi_{bi}+V_{FB1}-\frac{qN_D}{\varepsilon_s}\alpha^2+\frac{2}{t}\alpha^2\frac{q}{\varepsilon_s}\frac{1}{4p_4{}^2}(p_2-p_{c1})^2-\frac{2}{t}\alpha^2\frac{q}{\varepsilon_s}\frac{V_{FB1}}{p_4}(1-\frac{p_2}{p_{c1}})-P \tag{73}$$

Threshold voltage of this device can be expressed by the following equation by using Eq. (63) – (73),

$$V_{th}=\frac{-E+\sqrt{E^2-4DF}}{2D} \tag{74}$$

3.6 Simulation Methodology:

The results of the proposed analytical model have been validated by comparing with the outcomes obtained from a simulation model developed with Silvaco International's software package. An input deck was generated in the DECKBUILD™ VWF interactive tool, solved through the ATLAS™ routine, and analyzed utilizing the TONYPLOT™ tool. Additionally, the BLAZE™ routine, a routine specifically designed for group III-V materials and devices with position dependent band structures was utilized to simulate the AlGaN/GaN HEMT. The models developed to simulate the operation of semiconductor devices consist of equations derived from Maxwell's laws, Poisson's equation, the continuity equations and the drift-diffusion transport equations [71].

CHAPTER FOUR

THERMAL MODELING

4.1 Self-Heating Issue in AlGaN/GaN HEMT :

Self-heating is a major concern for AlGaN/GaN HEMT to be used in high power and high frequency applications. Hotspots are formed near the conducting channel because of increase in temperature and non-uniform circulation of dissipated power which ultimately deteriorates drain current and output power. Though large bandgap, high carrier velocity and large breakdown electric field have made AlGaN/GaN HEMT capable to operate at high power density, Joule heating becomes significant at high power levels which results in degraded performance of the device. High temperature of the devices during operation causes rapid reduction of mean time to failure (MITF) [72]. Various experimental [73], analytical [30] and simulation [74] techniques have been developed to study the effect of self-heating in SMG AlGaN/GaN HEMT. But to the best of our knowledge, still no analysis has been performed to investigate self-heating effect for DMG and TMG AlGaN/GaN HEMT. In this thesis, Finite Element (FE) method is utilized to explore the effects that self-heating employs in TMG HEMT using COMSOL multiphysics software, a dependable tool for HEMT analysis [73, 75]

4.2 Thermal Modeling:

The structure of TMG AlGaN/GaN HEMT used in the simulation consists of a 100 nm AlGaN layer on top of a 600 nm GaN layer on top of a 200 μm silicon carbide (SiC) layer which acts as the substrate. Drain and source metal contacts are made of copper (Cu), gate contact is composed of three different materials: nickel (Ni), iron (Fe) and tungsten (W). Thickness of drain, gate and source electrodes are 20 nm. Electrical and thermal conductivity of different materials used in the simulation are given in table 4.1. The bottom of SiC substrate is kept at a constant temperature of 300 K (works as a heat sink) and other external boundaries are considered to be adiabatic.

In Joule heating, resistive heating is initiated during the flow of electric current which causes increase of temperature. The generated resistive heat Q is proportional to the magnitude of the electric current density, J and is expressed as

$$Q \propto |J|^2 \tag{75}$$

J is proportional to the electric field, E which is found from the negative gradient of electric potential, V.

$$E = -\nabla V \tag{76}$$

Again, Eq. (75) can be written using a constant of proportionality, ρ as

$$Q = \rho |J|^2 = \frac{1}{\sigma} |\sigma E|^2 = \sigma |\nabla V|^2 \tag{77}$$

where ρ is the electric resistivity and the reciprocal of the temperature dependent electric conductivity, σ. The relationship between σ and temperature, T is given by

$$\sigma = \frac{\sigma_0}{1 + \alpha_T (T - T_0)} \tag{78}$$

where σ_0 is the conductivity at the reference temperature (T_0) and α_T is the temperature coefficient of resistivity.

Fourier's law of heat conduction is numerically solved by using finite element method and the temperature distribution profile is obtained throughout the device.

$$-\nabla.(k\nabla T) = Q \tag{79}$$

where k is the thermal conductivity and Q is the heat source, obtained from Eq. (77).

Table 4.1 Electrical and thermal conductivity of different materials used in thermal simulation

Material	Electrical conductivity (S/m)	Thermal conductivity (W/m.K)
Ni	1.43×10^7	91
Fe	1.00×10^7	80
W	1.79×10^7	174
Cu	5.96×10^7	401
AlGaN	556	50
GaN	1200	130
SiC	650	490

CHAPTER FIVE

RESULTS AND DISCUSSION

In this chapter, the results found from the proposed analytical model have been represented graphically and validated by comparing with the simulated characteristics obtained from commercially available 2D device simulator. Different design parameters used in both analytical and simulation study are listed in Table 5.1. In the following sections of this chapter, the obtained results from model and device simulator have been analyzed.

Table 5.1 Model Parameters

Parameters	Symbol	Value
Barrier layer doping density	N_D	10^{23} (m^{-3})
Source/Drain doping concentration	N_{D+}	10^{26} (m^{-3})
Intrinsic carrier concentration	N_i	10^{-4} (m^{-3})
Barrier layer thickness	t_b	25 (nm)
Spacer layer thickness	t_s	5 (nm)
Total thickness of AlGaN layer	$t = t_b+t_s$	30 (nm)
Ratio of individual metal gate lengths	$L_1:L_2:L_3$	1:1:1
Effective channel length	$L = L_1+L_2+L_3$	120 (nm)
Metal work function of region I, region II and region III	Φ_{M1}, Φ_{M2}, Φ_{M3} ($\Phi_{M1} > \Phi_{M2} > \Phi_{M3}$)	5 eV (Ni), 4.7 eV (Fe), 4.4 eV (W)
Electron charge	q	1.6×10^{-19} (C)
Temperature	T	300K

5.1 Channel Potential along the Channel:

5.1.1 Comparison among Various Device Structures:

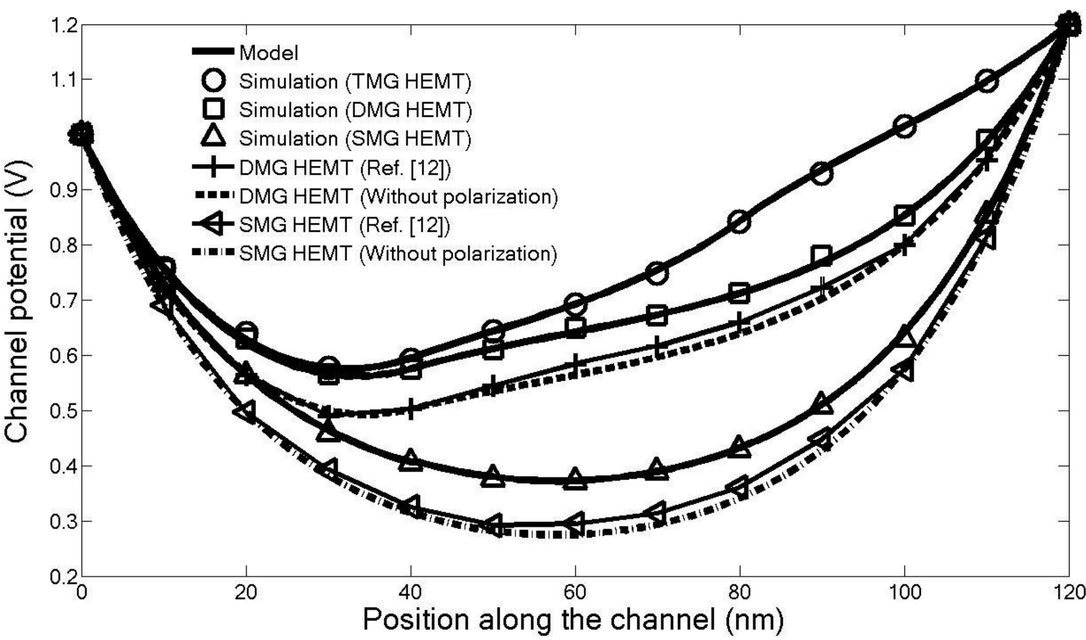

Fig. 5.1.1 Channel potential distribution along the channel position for SMG, DMG and TMG HEMT at V_{gs} = -0.2V, V_{ds} = 0.2V, L_1:L_2:L_3 = 1:1:1 for TMG HEMT

Fig 5.1.1 presents the channel potential of different structures along the channel position. The figure shows that TMG HEMT has the smallest slope channel potential curve among the three at the drain end which means the TMG structure suffers from least amount of hot carrier effect. Furthermore, there are two steps in channel potential profile of TMG HEMT compared to only one step and no step in DMG and SMG HEMT respectively. The steps are the results of work function difference among the gate materials. More step changes confirm improved screening of the area under the control gate (channel region under M1) from the drain to source voltage, V_{ds}. The figure also demonstrates a fine agreement between the results obtained from our model and the model developed by Kumar *et al.* [12] for SMG and DMG HEMT without including polarization effect.

5.1.2 Effect of Ratio of Individual Metal Gate Length:

Channel potential profile is depicted in Fig 5.1.2 for three different combinations of L_1, L_2 and

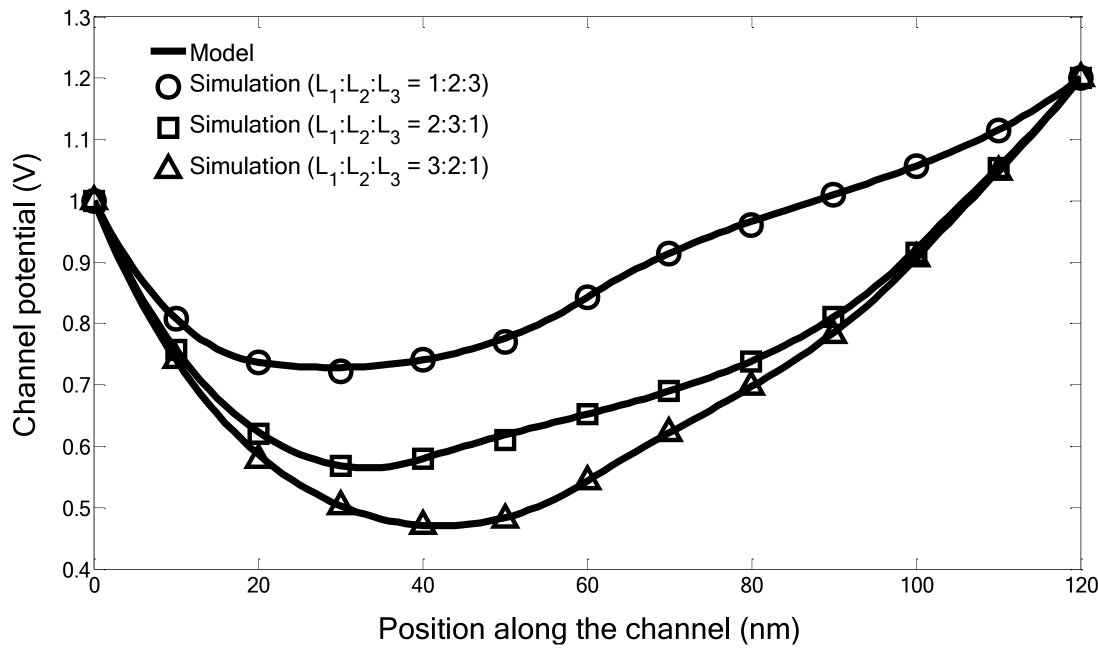

Fig. 5.1.2 Channel potential profile of TMG HEMT along the position of the channel for various metal gate length (L_1, L_2 and L_3) ratios

L_3 keeping the total channel length, L constant. The channel length under the control gate (L_1) is considered to be 20nm, 40nm and 60nm while the ratios of L_1, L_2 and L_3 are equal to 1:2:3; 2:3:1 and 3:2:1, respectively for L = 120nm. The figure evidently discloses the fact that with the decrease of L_1, minimum channel potential increases which causes lowering of potential barrier and decrease of threshold voltage. Thus subthreshold current will increase with the smaller L_1. Another fact is that, as L_1 reduces, position of channel potential minima gradually shifts towards the source end and hence decreases the influence of drain to source voltage on the channel. Therefore, less amount of L_1 reduces DIBL effect significantly. So an optimized ratio of control and screen gates is necessary to obtain a reasonable tradeoff between subthreshold current and DIBL.

5.1.3 Variation with Total Channel Length:

Fig 5.1.3 demonstrates the effect of different channel lengths on channel potential variation along the channel position. Minimum channel potential rises with the decrease in channel length. Thus the channel barrier becomes smaller and short channel effects become significant.

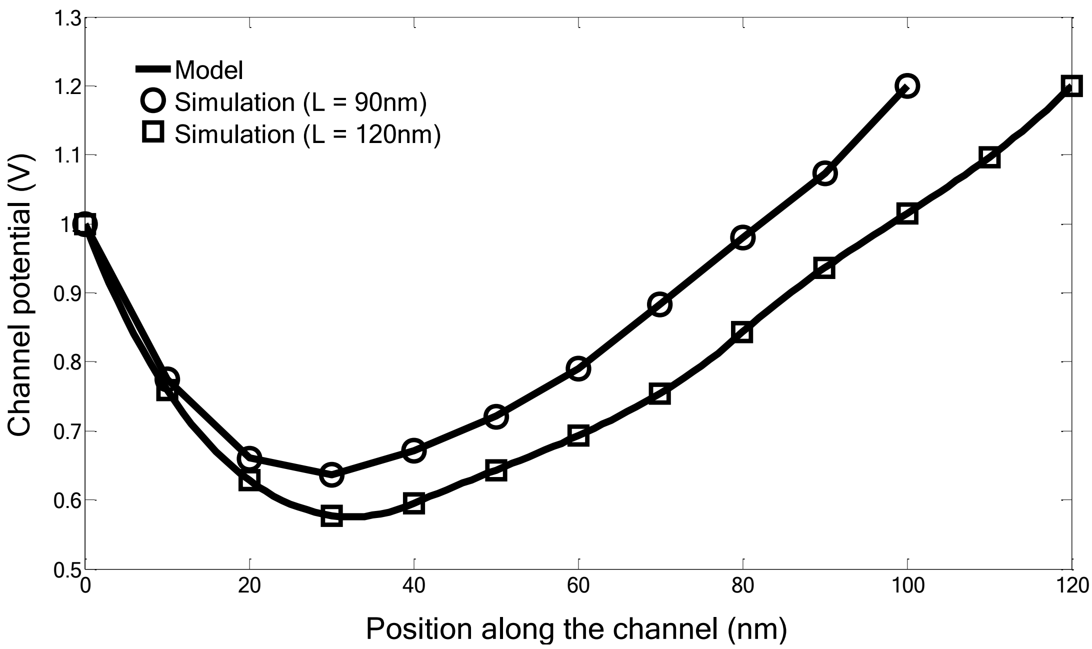

Fig. 5.1.3 Variation in channel potential with the channel position for different values of total channel lengths considering $L_1:L_2:L_3 = 1:1:1$

5.1.4 Effect of Drain Bias:

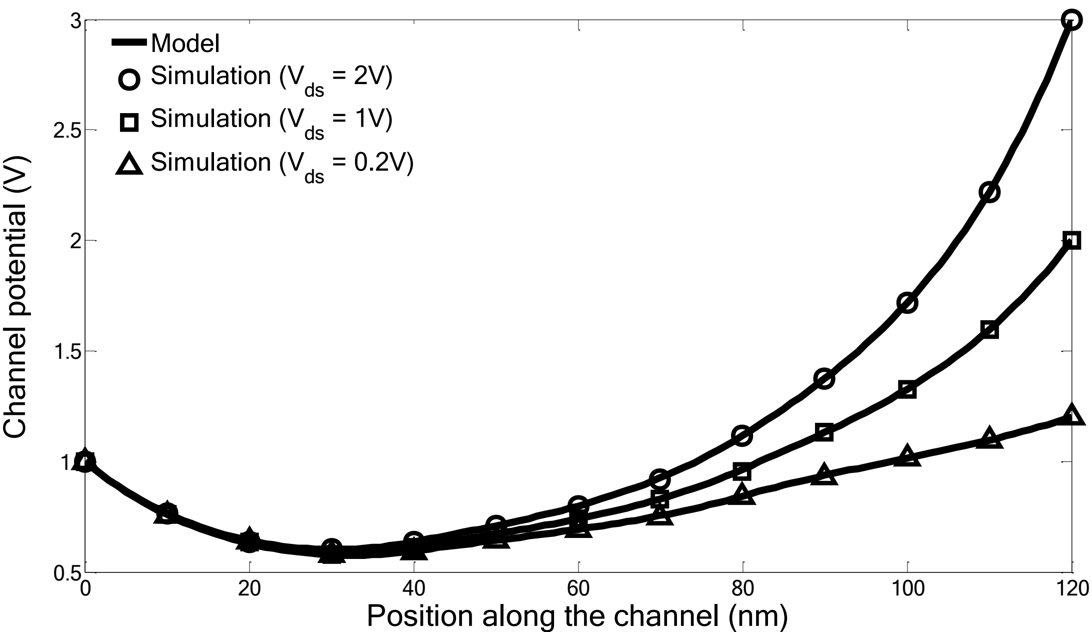

Fig. 5.1.4 Channel potential variation with channel position for different drain to source voltages

Fig 5.1.4 presents channel potential distribution in TMG structure as a function of drain to

source voltages. For various V_{ds}, it is clear from the figure that, there is negligible change in potential under M1 region while potential under M2 and M3 regions face significant change. That means potential drop in the region under the control gate, M1 is screened by the two screen gates M2 and M3 from the variations in drain voltage. For larger V_{ds} , minimum value of channel potential increases which leads to the reduction in potential barrier and enhancement of carrier transport efficiency at the expense of significant DIBL effect.

5.1.5 Variation with Barrier Layer Doping Concentration:

Channel potential variation along the channel for various doping concentration of AlGaN barrier layer is presented in Fig 5.1.5. Increase in doping concentration means more amount of electrons being diffused from AlGaN to GaN which adds to the 2DEG density at the AlGaN/GaN interface. As a result, sheet carrier concentration of 2DEG channel increases which yields a reduction in the channel potential barrier. Fig 5.1.5 clearly testifies this fact.

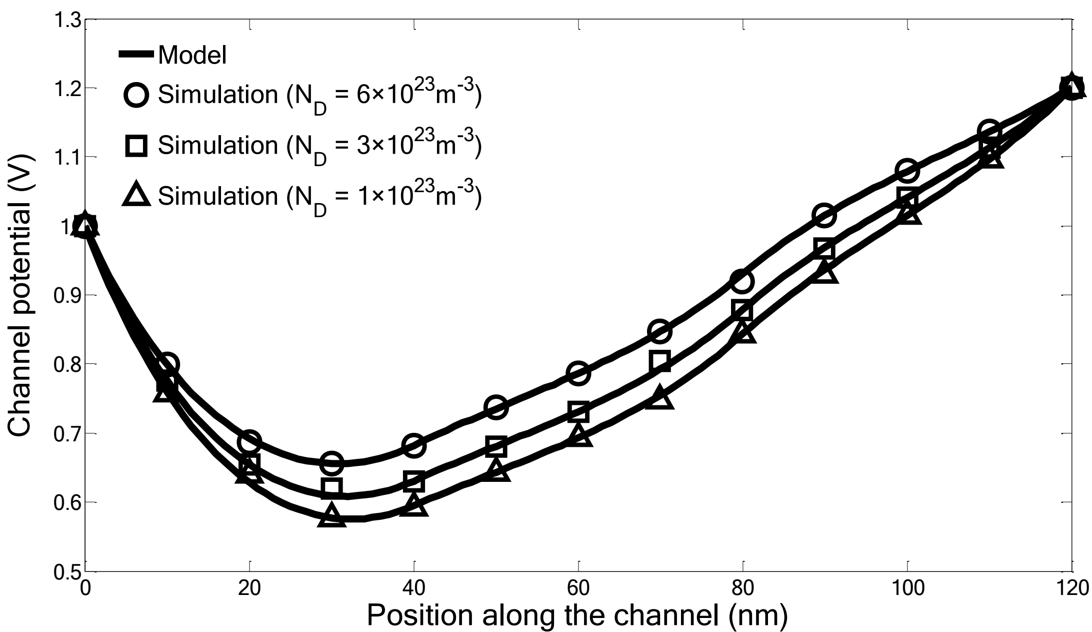

Fig. 5.1.5 Change in channel potential with lateral position along the channel for various doping concentration of AlGaN barrier layer

5.1.6 Changes with Mole Fraction of Al in AlGaN:

Variation of channel potential with channel position for different Al mole fraction (m) in $Al_mGa_{1-m}N$ is presented in fig 5.1.6. Large value of Al composition results in an increase in bandgap of AlGaN [69]. As a result, conduction band offset at the AlGaN/GaN heterojunction is increased and more carriers get confined at the heterointerface. Consequently, sheet carrier concentration at the 2DEG channel is increased and source channel barrier height gets reduced which is shown in the figure.

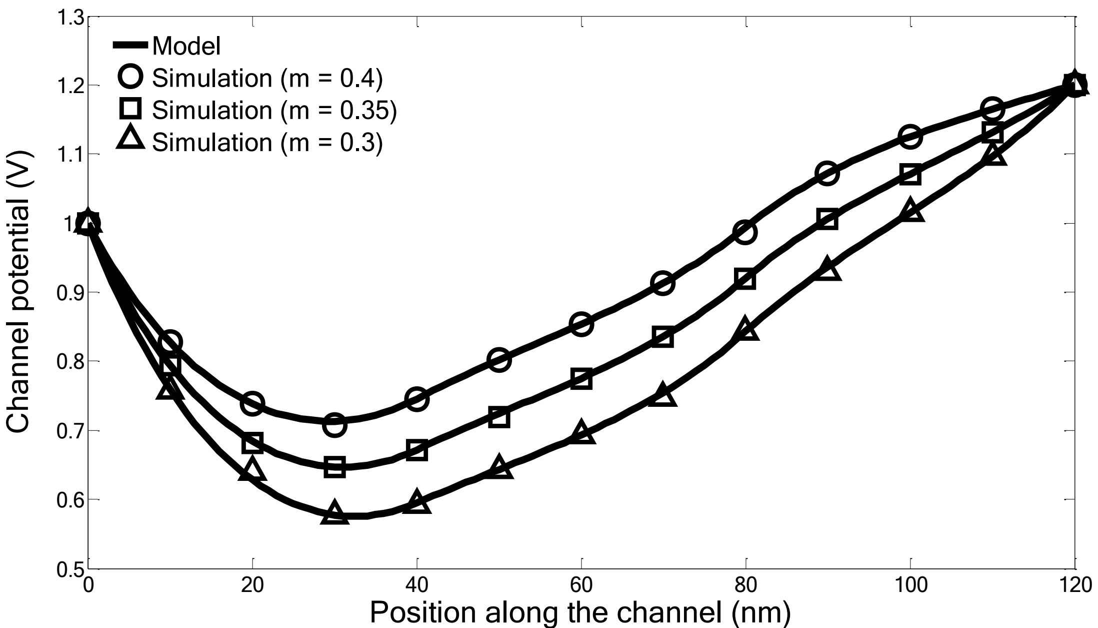

Fig. 5.1.6 Variation in channel potential profile versus lateral position along the channel for different mole fraction values of Al in AlGaN

5.1.7 Effect of Barrier Layer Thickness:

Fig 5.1.7 shows channel potential distribution along the position of the channel for different AlGaN barrier layer thickness, t_b. Channel potential barrier decreases with the increase in t_b as shown in the figure. As previously described, increase in t_b results in a rise in sheet carrier density at the AlGaN/GaN heterointerface. Therefore, due to the increase in 2DEG concentration, channel potential minima increases and channel potential barrier becomes lower.

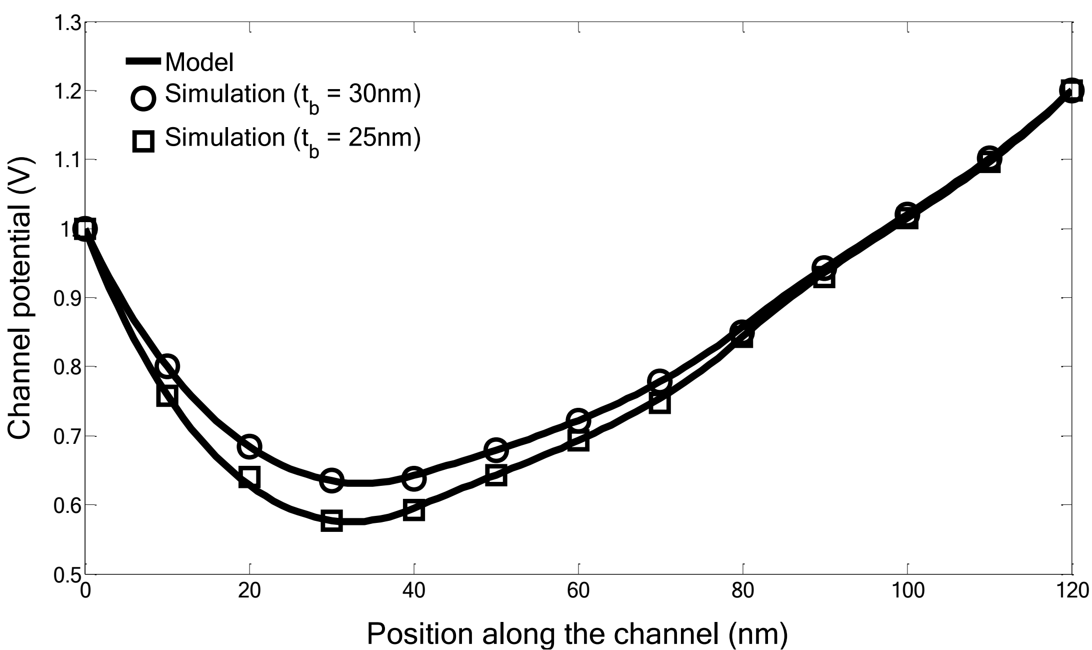

Fig. 5.1.7 Shift of channel potential with lateral position along the channel for different thickness of AlGaN barrier layer

5.1.8 Minimum Channel Potential: Impact of Total Channel Length:

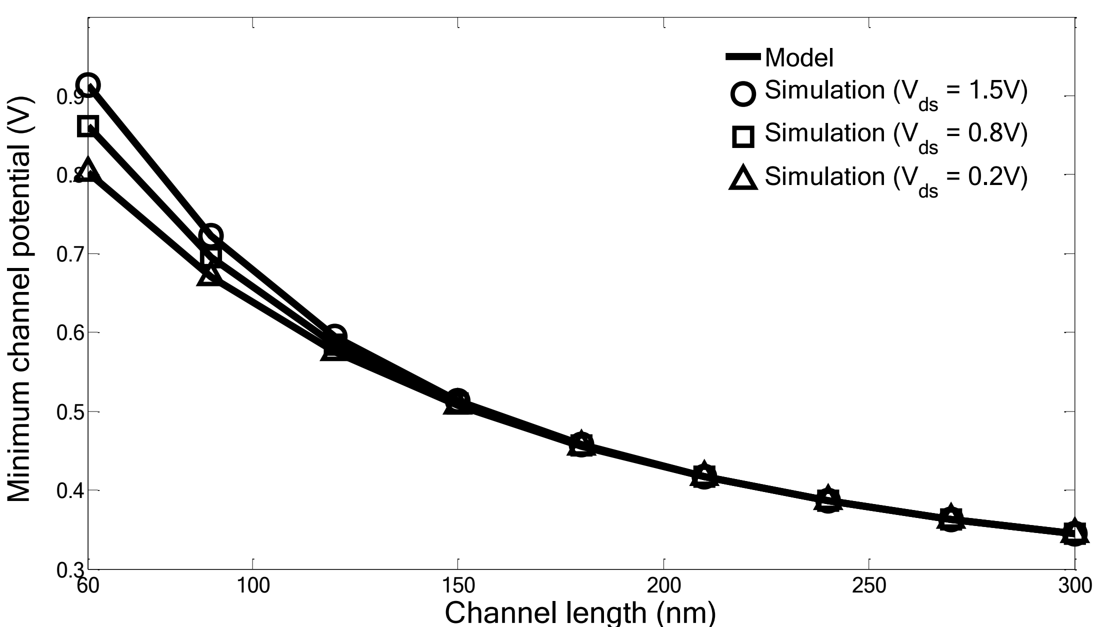

Fig. 5.1.8 Minimum channel potential against total channel length for different drain to source voltages

Variation in minimum channel potential with total channel length keeping the L_1, L_2 and L_3

ratio same is presented in Fig 5.1.8. Reduction in channel length causes large amount of electric flux to enter the source from drain end. Thus channel potential minima increases and this increase is more pronounced for channel lengths less than 150 nm. Minimum channel potential increases with the increase in V_{ds} due to rise in electric field. For larger channel lengths, drain terminal has very little control on the channel and thus channel potential minima becomes independent of V_{ds} values which is observed in the figure.

5.1.9 Polarization Effect:

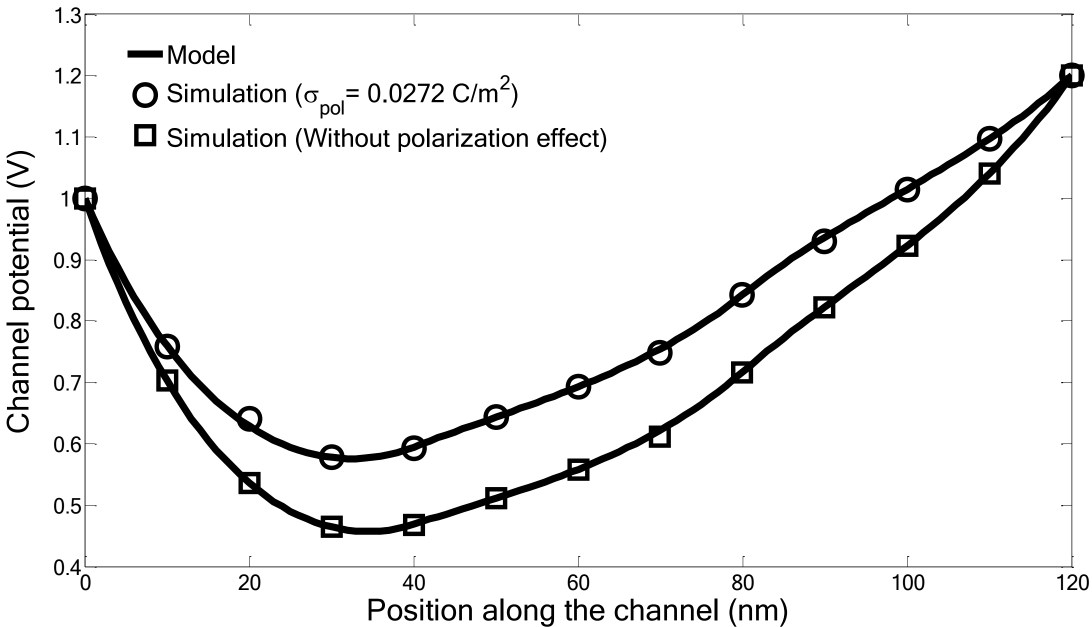

Fig. 5.1.9 Channel potential as a function of lateral position along the channel with and without polarization effect

Impact of polarization on channel potential along channel position is shown in Fig 5.1.9. The upper curve represents channel potential distribution with polarization induced charge density of 0.0272 C/m^2 while the lower curve is found without considering polarization effect. The figure signifies that, minimum channel potential increases in presence of polarization effect. Spontaneous and piezoelectric polarization induced charges contribute to the sheet carrier concentration in 2DEG channel. This high sheet charge density leads to rise in channel potential and decrease in channel potential barrier. Device current increases as a result of reduced channel barrier height.

5.1.10 Effect of Trapped Charge:

Fig 5.1.10 illustrates the trapped charge effect on channel potential. As trapped charge results in reduction of mobile carriers in the channel formed by 2DEG, channel potential minima decreases with electron trapping and therefore, channel potential barrier is increased which ultimately causes the decrease in current. This effect becomes large with the increase in trapped charge.

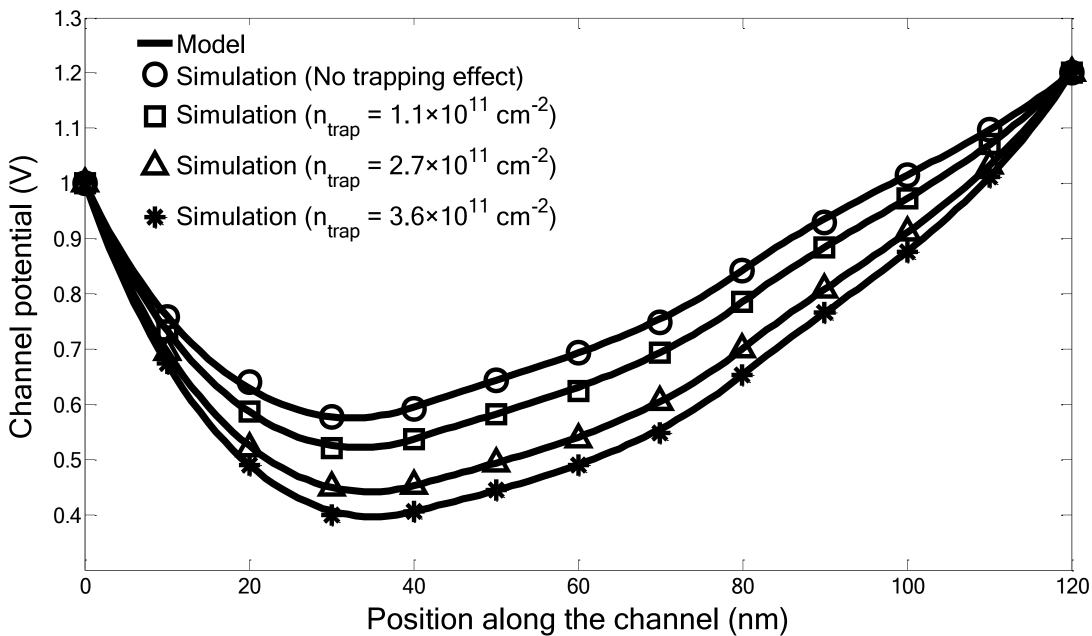

Fig. 5.1.10 Channel potential profile along channel position with different amount of trapped charge

5.2 Electric Field along the Channel:

5.2.1 Comparison among Various Device Structures:

Fig 5.2.1 presents the electric field profile of TMG, DMG and SMG HEMTs along the position of the channel. Electric field profile of TMG HEMT exhibits two peaks whereas there appears a single peak and no peak for DMG and SMG HEMT, respectively. The peaks actually occur at the interface of two gate metals with different work functions which increase the average electric field in the channel. Electron transport velocity is increased because of this enhancement of the average field. Another fact, clearly visible from the figure is that, the peak electric field at the drain end has the smallest magnitude for TMG HEMT compared to DMG

and SMG HEMT due to having gate metal with the smallest work function near the drain end. Therefore, TMG structure suffers from least amount of hot carrier effects. Thus impact ionization also gets reduced and results in enhancement of breakdown voltage.

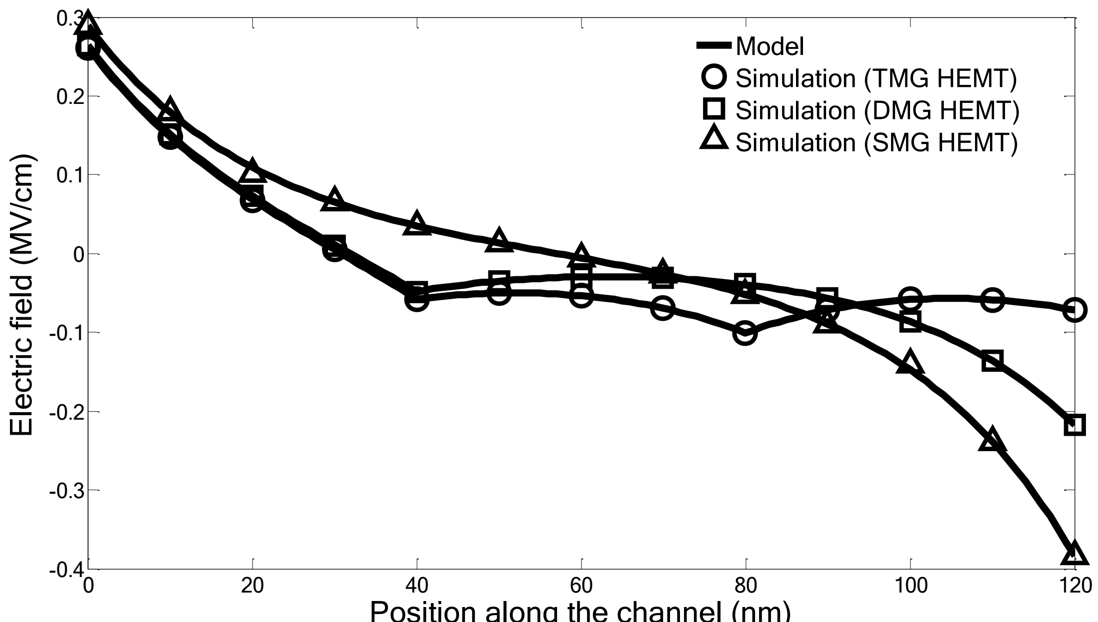

Fig. 5.2.1 Variation in electric field with lateral position of the channel for SMG, DMG and TMG HEMT

5.2.2 Effect of Ratio of Individual Metal Gate Length:

Fig 5.2.2 shows the longitudinal electric field along the channel position for three different combinations of length of individual metal gates i.e. different ratio of L_1, L_2 and L_3. Decrease of L_1 results in a more even allocation of electric field in the channel as the electric field peak is shifted towards the source end. It can be observed from the figure that peak electric field at the drain terminal is the minimum for TMG structure with 1:2:3 ratio of L_1, L_2 and L_3. Hence this particular structure is least prone to hot carrier effects causing enhanced device lifetime.

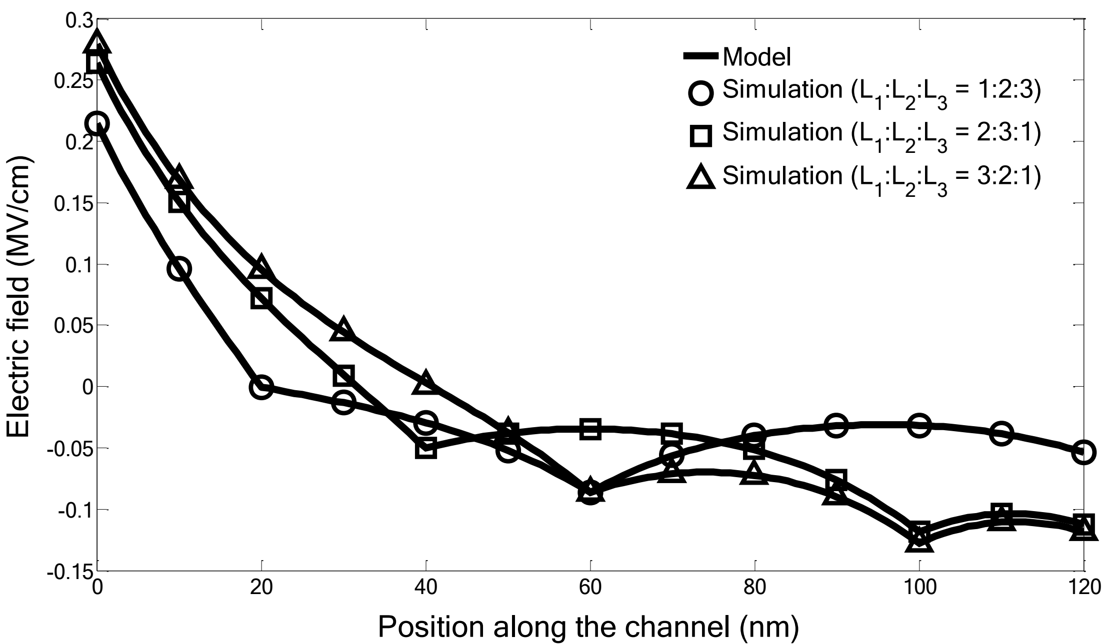

Fig. 5.2.2 Electric field variation with position along the channel of TMG HEMT for different ratio of L_1, L_2 and L_3

5.2.3 Variation with Drain Bias:

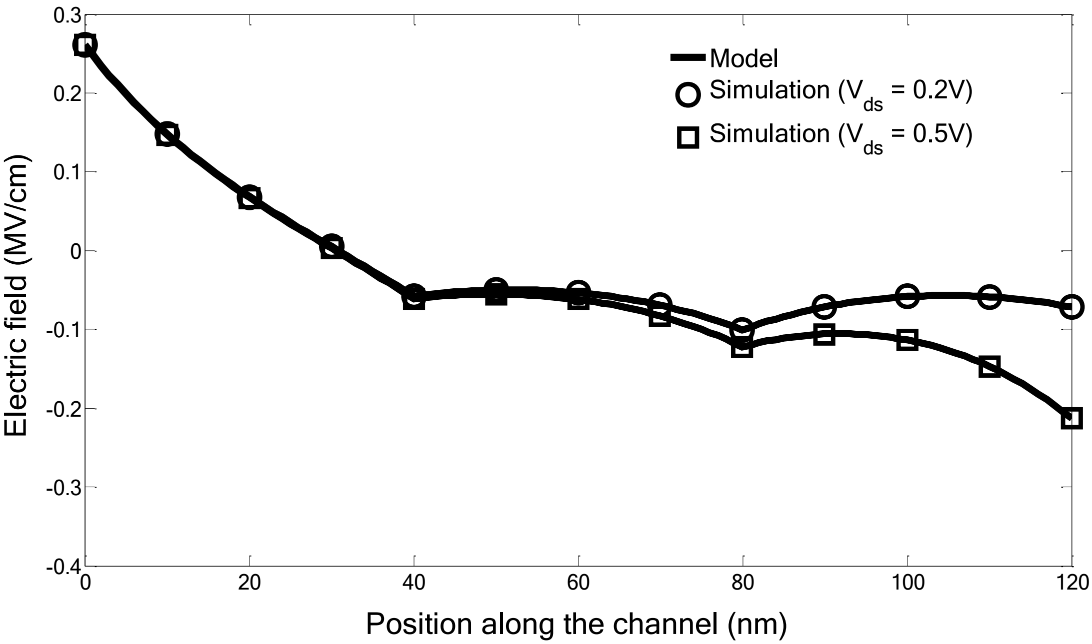

Fig. 5.2.3 Electric field profile along channel position for different drain to source voltages

The electric field dependency on drain to source voltages, V_{ds} along the channel position is presented in Fig 5.2.3. The plot reveals that peak electric field at the drain end increases with the rise of V_{ds} for constant V_{gs} resulting in boost of hot carrier effect.

5.2.4 Polarization Effect:

Effect of polarization on the distribution of electric field along the channel is presented in Fig 5.2.4. Electric field is found to be smaller at the drain terminal due to the presence of polarization effect which leads to reduced hot carrier effect and improved device lifetime.

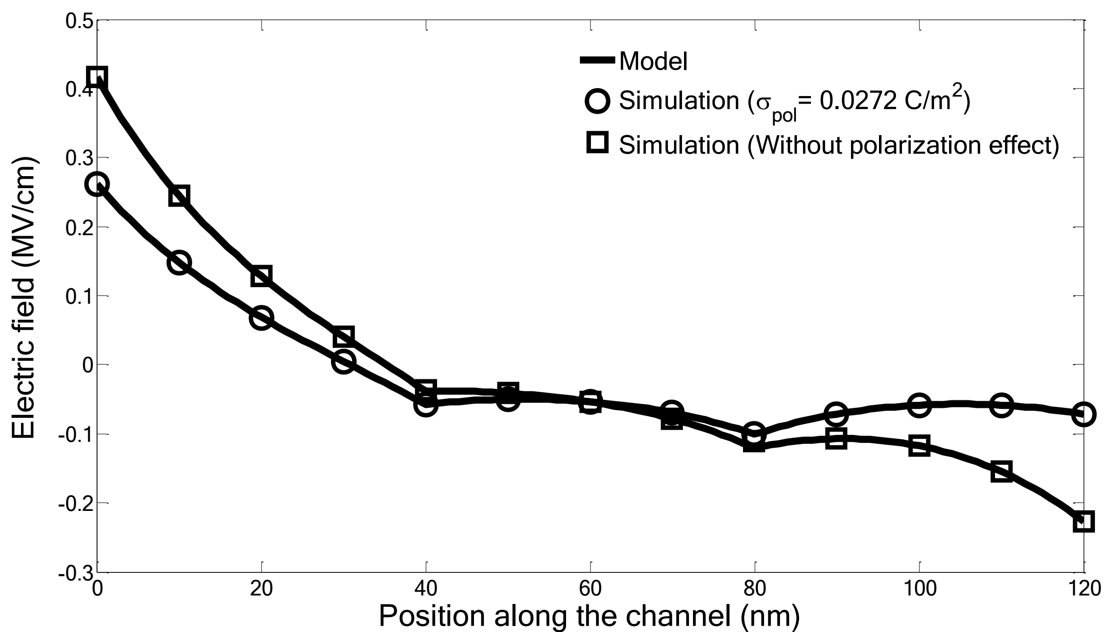

Fig. 5.2.4 Effect of polarization on electric field distribution along the channel

5.3 Threshold Voltage:

5.3.1 Effect of Barrier Layer Thickness:

AlGaN/GaN HEMT structure developed in this thesis is a depletion mode device since it is more natural due to its polarization property. So the device is naturally conductive if no voltage is applied between gate and source. To turn off the device, a negative V_{gs} (known as the threshold voltage) is applied so that the electrons under the gate area is depleted. Hence, threshold voltage is found to be negative for the proposed structure. Fig 5.3.1 shows the

variation of threshold voltage (V_{th}) with total channel length (L) for different thickness of AlGaN barrier layer (t_b). The figure clearly shows that for both values of t_b, variation of V_{th} is very small at higher channel lengths whereas there is a roll-off of the threshold voltage values for smaller channel lengths. For the same channel length, V_{th} is found to be smaller for thicker AlGaN barrier layer due to its higher channel potential minima as observed in Fig. 5.1.7.

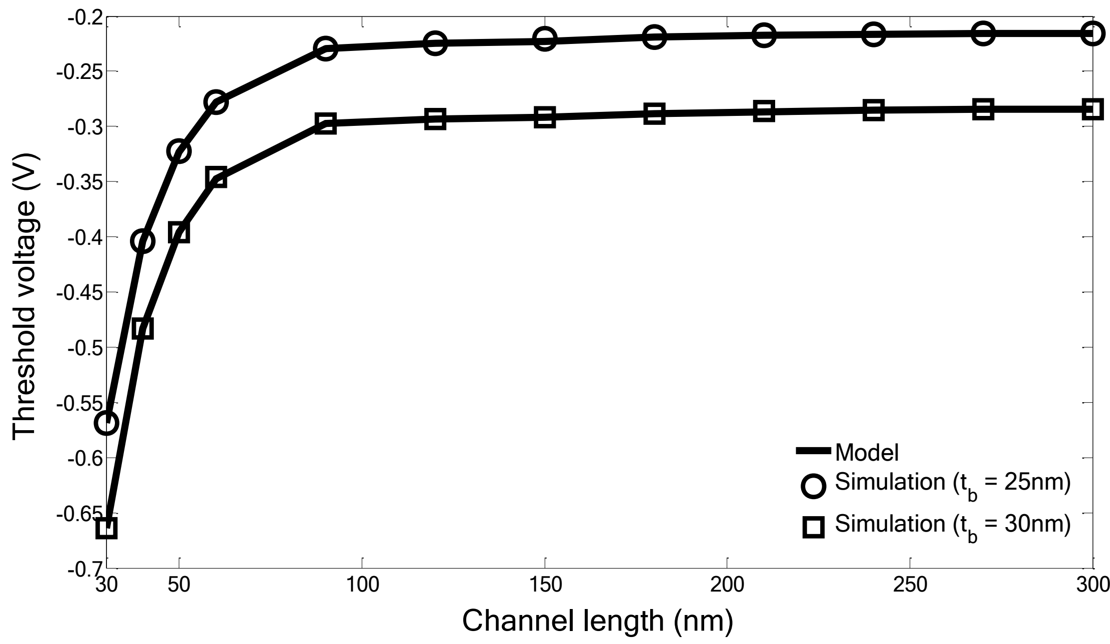

Fig. 5.3.1. Threshold voltage variation of TMG HEMT with lateral position along the channel for different values of t_b

5.3.2 Variation with Total Channel Length:

The drain to source voltage dependence of threshold voltage for various channel lengths is illustrated in Fig 5.3.2. V_{th} is almost independent of V_{ds} for larger channel length (L = 240 nm). Effect of V_{ds} on the control gate becomes larger for short channel and more amount of electric flux enters into the channel from the drain terminal. Consequently, source channel barrier gets lower and DIBL effect becomes significant which causes a reduction in the V_{th} with the increase in V_{ds}. Fig 5.3.2 clearly signifies the fact for both simulation and analytical model outcomes.

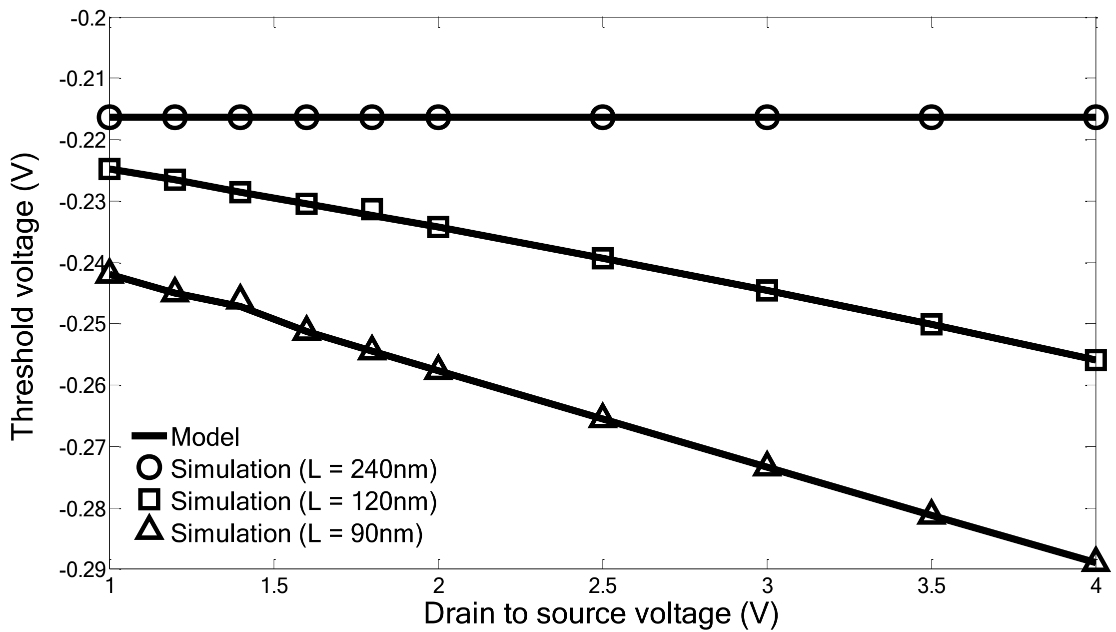

Fig. 5.3.2 Threshold voltage distribution with drain to source voltage for various total channel lengths

5.3.3 Changes with Ratio of Individual Metal Gate Length:

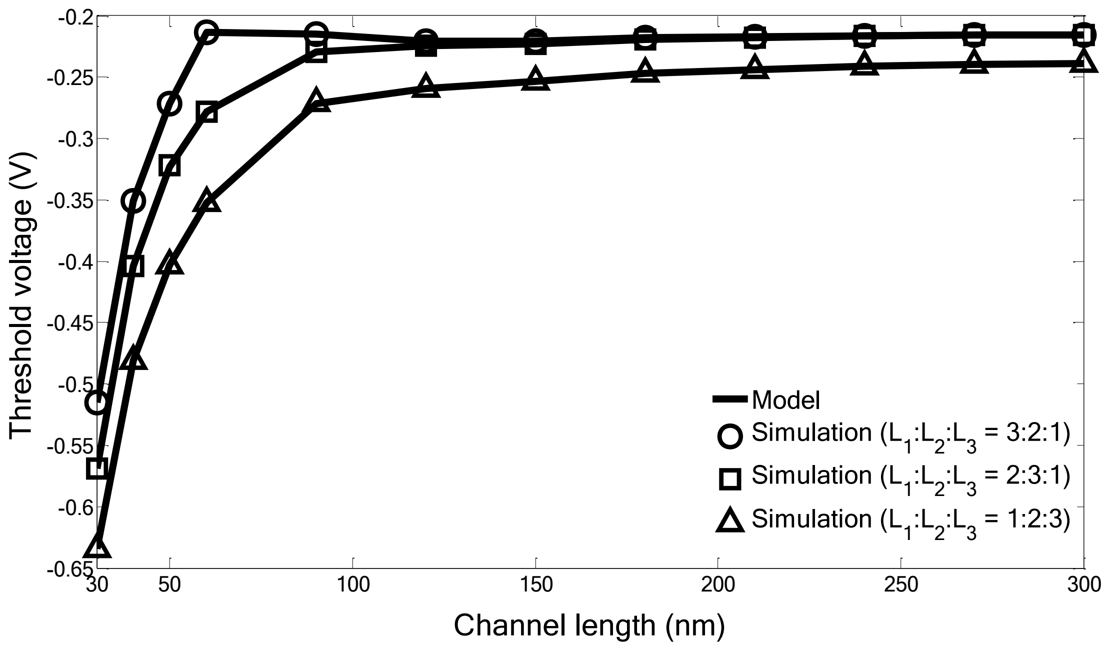

Fig. 5.3.3 Threshold voltage versus total channel length for different metal gate length ratios

Effect of ratio of individual metal gate lengths on threshold voltage for various total channel

lengths is given in Fig 5.3.3. Channel potential minima decreases and as a result, channel potential barrier becomes larger with the increase in length of the control gate (L_1). Threshold voltage value thus gets higher with larger L_1 (increased L_1:L_2:L_3). Threshold voltage roll off is found to be smaller for high L_1 value. The figure also depicts that device with longest control gate (3:2:1 ratio of L_1, L_2 and L_3) of L=60 nm experience the reverse short channel effect.

5.3.4 Effect of Drain Bias:

Fig 5.3.4 represents the impact of drain to source voltages on threshold voltage at various channel length. Threshold voltage gets lower with the increase in drain bias because of greater amount of DIBL effect. As DIBL effect gets reduced for a large channel, the threshold voltage becomes almost independent of drain to source potential for long channel lengths.

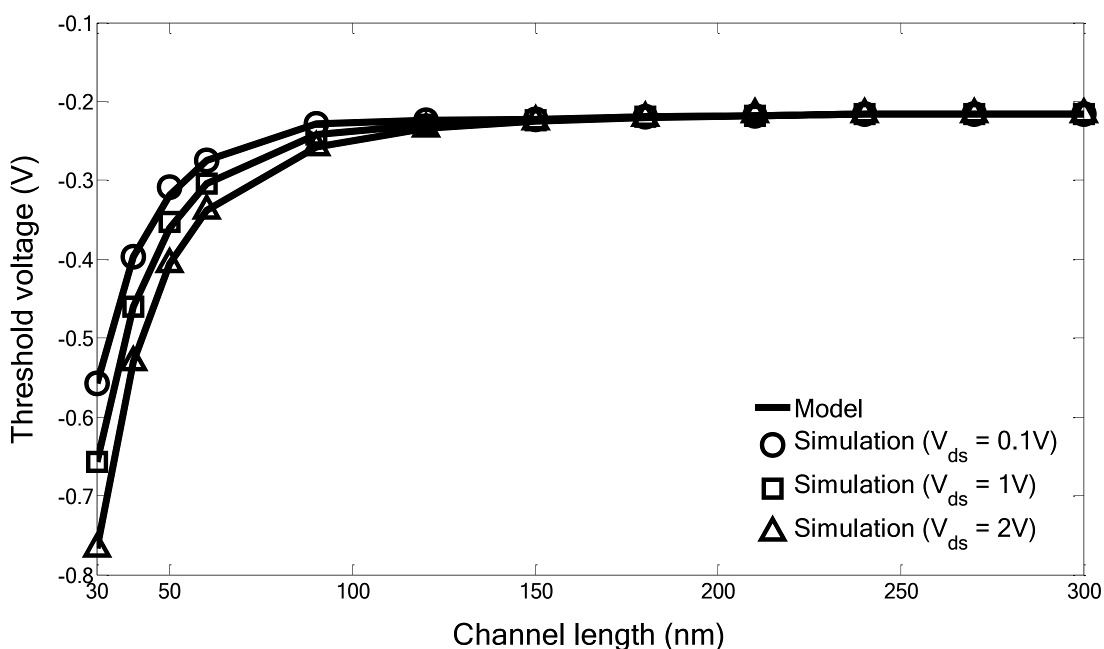

Fig. 5.3.4 Variation in threshold voltage with total channel length for various drain to source voltages

5.3.5 Comparison among Various Device Structures:

A comparison among threshold voltage values of SMG, DMG and TMG HEMT is represented in Fig. 5.3.5 for different channel lengths. TMG HEMT needs less voltage to be turned on i.e. lower threshold voltage in comparison with DMG and SMG HEMT. Because of this, TMG

structure can minimize power dissipation and thus this type of HEMT can be used in low power circuits.

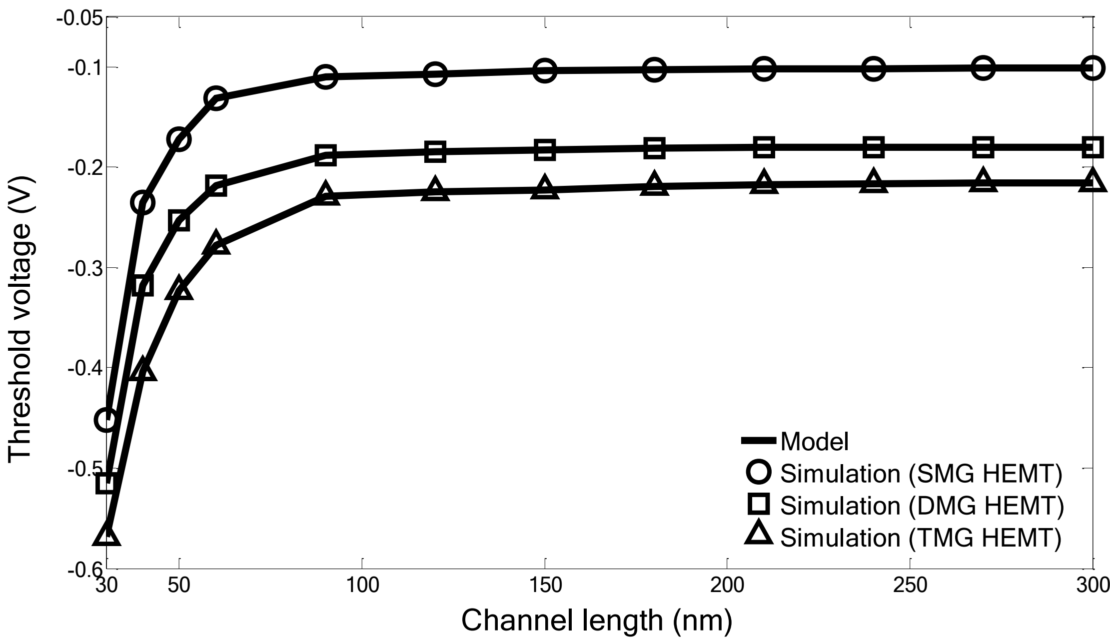

Fig. 5.3.5 Change in threshold voltage with total channel length for SMG, DMG and TMG HEMT

5.4 Drain Induced Barrier Lowering (DIBL) Effect:

5.4.1 Comparison among Various Device Structures:

DIBL effect in case of TMG HEMT for different channel lengths is shown in Fig 5.4.1. DIBL is calculated from the following equation:

$$\mathrm{DIBL} = \frac{V_{th1} - V_{th2}}{V_{ds2} - V_{ds1}}$$

where V_{th1} and V_{th2} are threshold voltage of the device at drain voltages of $V_{ds1} = 0.1$V and $V_{ds2} = 1.1$V respectively. It is observed from the figure that, DIBL is larger for short channel devices whereas it is almost zero for long channel structures. Gate terminal gradually loses its control on the carriers along the channel with the decrease in channel lengths while drain gets more control on it. On the other hand, for a larger channel length, carrier transport along the channel is almost fully controlled by the gate terminal and very small influence of drain

terminal persists which results in a much reduced amount of DIBL effect. A comparison with DMG and SMG HEMTs in terms of DIBL is also shown in the figure. Due to having more screen gates than DMG and SMG structures, TMG HEMT provides better screening of the channel potential under the control gate region from variation in drain potential and therefore, suffers from less amount of DIBL effect.

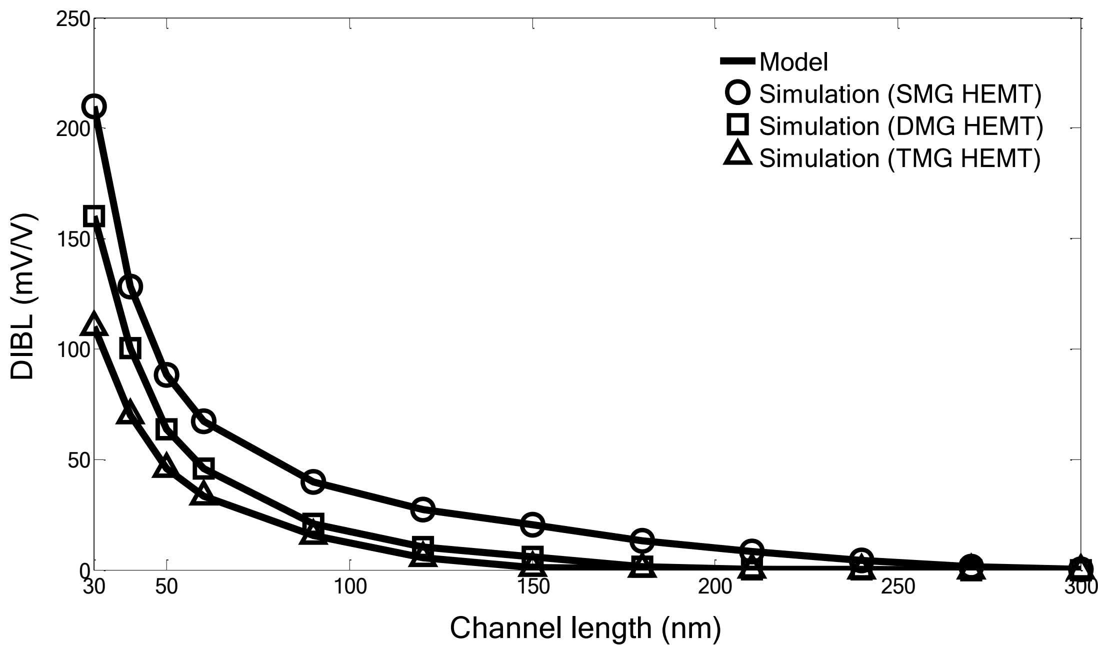

Fig. 5.4.1 DIBL vs total channel length for SMG, DMG and TMG HEMT structures

5.4.2 Influence of Ratio of Individual Metal Gate Length:

DIBL effect against different total channel lengths is plotted in Fig 5.4.2 for various individual gate length combinations (different ratio of L_1, L_2 and L_3). As seen from the figure, TMG HEMT with 1:2:3 ratio of L_1, L_2 and L_3 suffers from least amount of DIBL among the three structures. As stated earlier, control gate, M1 having gate length, L_1 is screened from variation in drain voltages by the screen gates, M2 and M3 having gate lengths of L_2 and L_3 respectively. Therefore, if length of the screen gates increase, effect of drain potential on the carriers in the channel is reduced due to screening phenomenon and better gate controllability is achieved. For larger channel lengths, DIBL effect becomes almost negligible and becomes independent of L_1, L_2 and L_3 ratio.

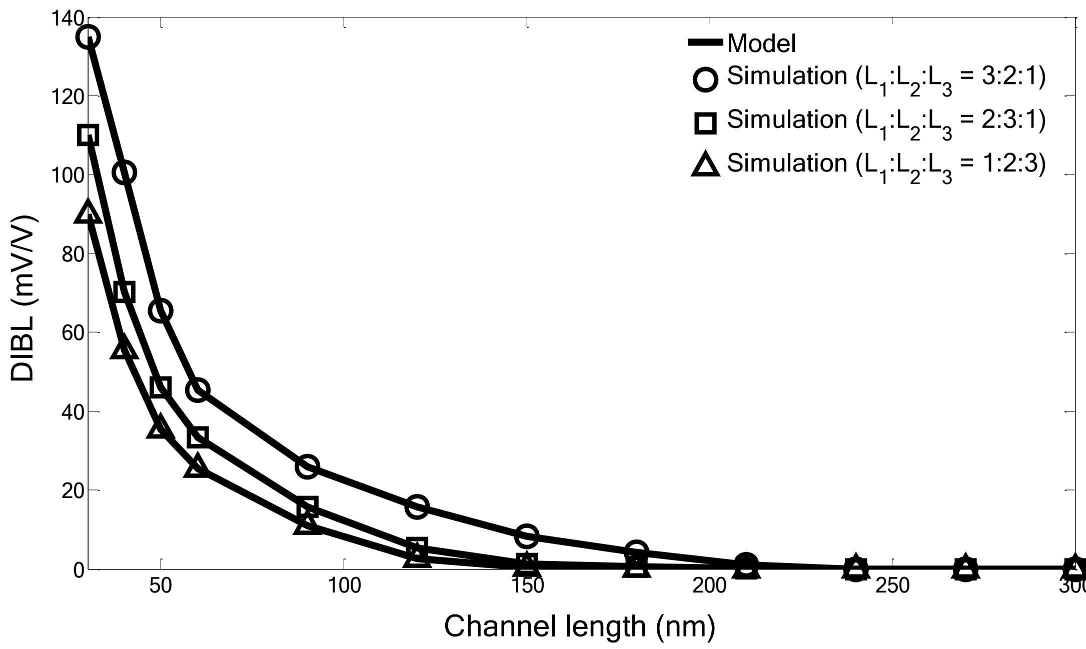

Fig. 5.4.2 Impact of different ratio of L_1, L_2 and L_3 on DIBL effect in TMG HEMT for various total channel lengths

5.5 Channel Temperature Due to Self-Heating Effect:

5.5.1 Temperature Profile across the Device: Comparison among Various Device Structures

Fig 5.5.1 displays the temperature distribution profile in TMG HEMT. Finite element analysis using COMSOL Multiphysics software is performed to obtain the heat distribution profile throughout the device. The temperature rise in the device is an effect of self-heating phenomena generated from current flow. Table 5.2 shows maximum channel temperature generated in TMG, DMG and SMG HEMTs. Reduced source channel barrier height, enhanced carrier velocity along the channel and improved carrier transport efficiency will result in a higher drain to source current for TMG structure with respect to the DMG and SMG devices. Though greater amount of current will flow in TMG configuration, still temperature does not increase too much from the other two structures which is obvious from the table. So TMG HEMT provides both superior current carrying capability and better thermal performance.

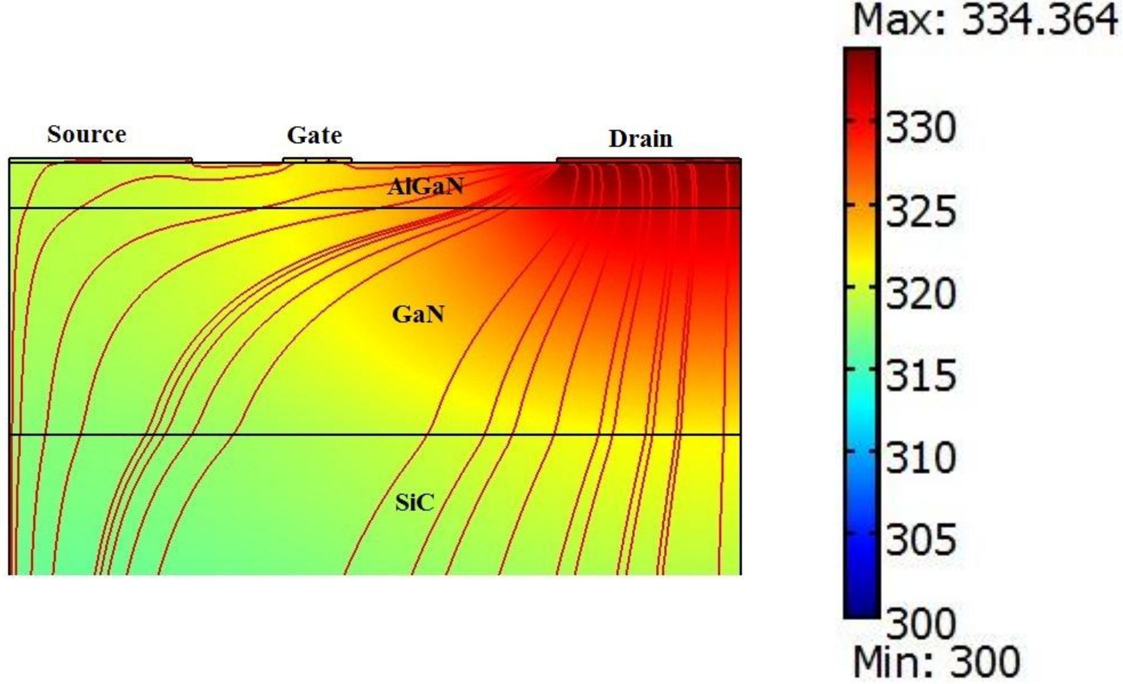

Fig. 5.5.1 Temperature distribution profile across the device for TMG HEMT with L_1:L_2:L_3 = 1:1:1, V_{ds} = 5V and V_{gs} = -0.2V

Table 5.2 Maximum channel temperature for TMG, DMG and SMG HEMT

Structure	Maximum Channel Temperature (K)
TMG HEMT	334.364
DMG HEMT	332.354
SMG HEMT	329.348

5.5.2 Effect of Drain and Gate Biases:

Fig 5.5.2 shows the impact of drain voltage and gate voltage on maximum temperature rise (T_{max}) in TMG HEMT. T_{max} in the device increases with the rise in drain potential. High drain voltage results in an increase in electric field across the channel which increases electron velocity. Accelerated electrons increase interaction with the crystal lattice and lead to temperature rise by releasing more energy through Joule heating. Increase in gate voltage results in an increase in 2DEG concentration leading to rise in current and therefore temperature gradually increases with increased Joule heating.

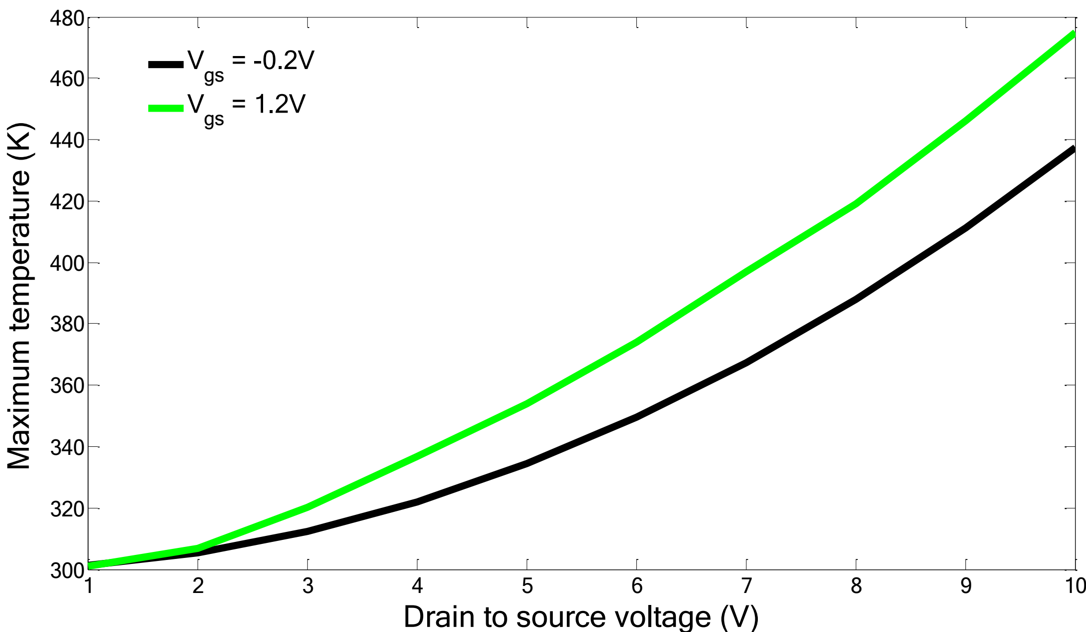

Fig. 5.5.2 Maximum temperature in TMG HEMT versus drain to source voltage, V_{ds} for different gate to source voltages, V_{gs}

5.5.3 Effect of AlGaN Layer Thickness:

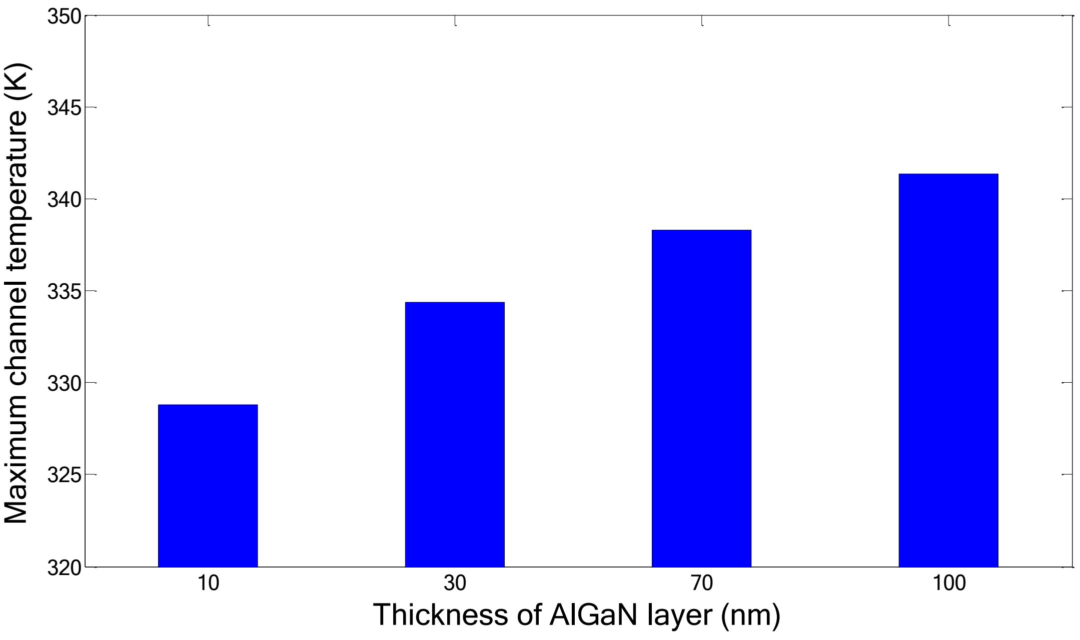

Fig. 5.5.3 Maximum channel temperature versus AlGaN layer thickness

Fig 5.5.3 shows that higher channel temperature is found in TMG HEMT with thick AlGaN Layer. As shown in Fig. 5.1.7, increase in barrier layer thickness results in reduced source-

channel barrier height and increase in current density. Thus, channel temperature will rise with increased Joule heating.

5.5.4 Impact of Ratio of Different Gate Metal Length:

Maximum channel temperature is shown in Fig 5.5.4 for various ratio of gate material lengths. Increased Joule heating effect resulting from higher current density is responsible for greater channel temperature in case of TMG HEMT with smaller control gate length (L_1). Higher current density is the consequence of minimized channel potential barrier which is explained with Fig 5.1.2.

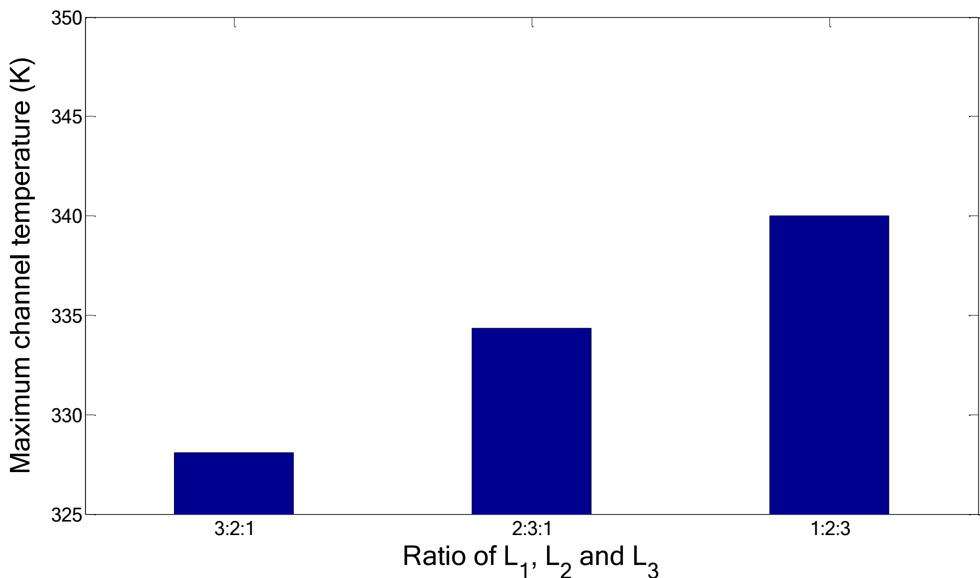

Fig. 5.5.4 Effect of ratio of gate metal lengths on maximum channel temperature. L_1 = 60 nm, 40 nm and 20 nm for L_1:L_2:L_3 = 3:2:1, 2:3:1 and 1:2:3 respectively for total channel length of 120 nm

5.5.5 Comparison Among Various Substrate Materials:

Fig 5.5.5 demonstrates the performance of four different substrate materials in terms of maximum channel temperature generated during device operation. Material with higher thermal conductivity effectively removes heat from the device and thus channel temperature rise gets reduced. Thermal conductivity of the four substrate materials in the figure is listed in

Table 2.2. Due to higher thermal conductivity, channel temperature is minimum for SiC and hence it can be used for better thermal performance of the device.

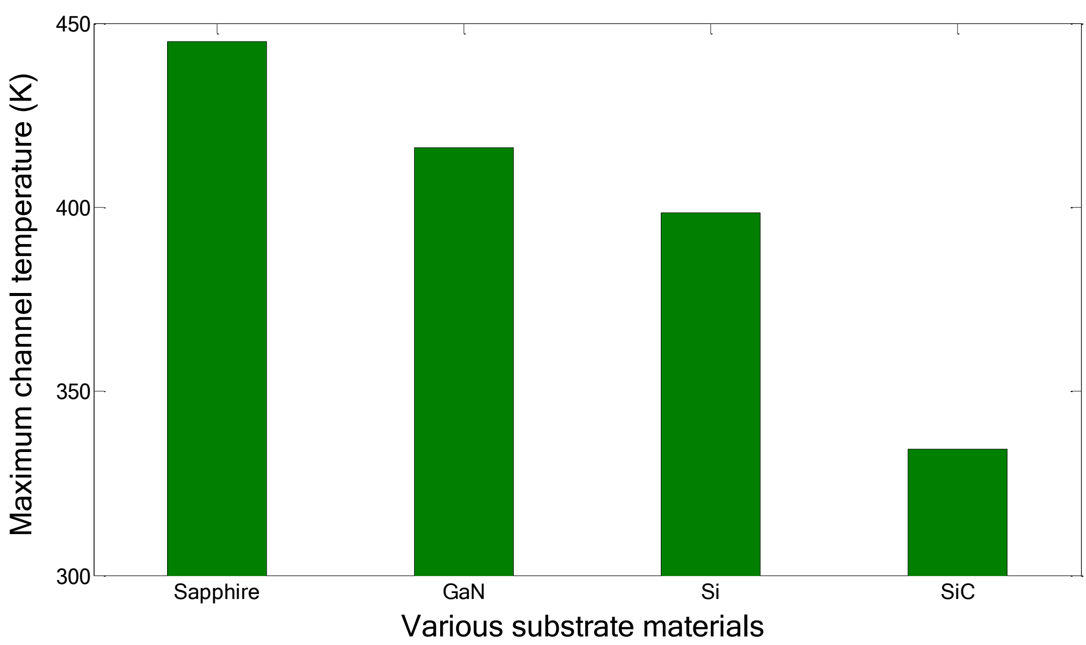

Fig. 5.5.5 Maximum channel temperature for various substrate materials

CHAPTER SIX

CONCLUSION

6.1 Conclusion:

Continuous miniaturization of HEMTs for the development of ultra high density ICs has resulted in degradation of device parameters by increasing short channel effects. Triple material gate HEMT is an excellent solution to this problem as it offers good performance parameters such as suppressed SCEs, efficient carrier transport and high speed operation. In this work, a two dimensional analytical model of triple material gate AlGaN/GaN HEMT has been presented. Gate material engineering technique has been employed in this structure by laterally connecting three materials having different work function to form the gate electrode. Two dimensional Poisson's equation with proper boundary conditions has been solved to derive the expression of channel potential using parabolic approximation procedure. Spontaneous and piezoelectric polarization induced charges have been incorporated in the model as they make significant contribution in 2DEG formation at the heterointerface. Temperature and mole fraction dependence of various device parameters have also been included to develop precise model of channel potential. Different work functions of the gate metals result in generating step function like channel potential profile with two steps which ensure better screening of the channel from drain potential and DIBL effect is thereby minimized. Expression of electric field has been derived by taking the first order spatial derivative of the channel potential. The study reveals the fact that electric field value at the drain end is much lower in TMG HEMT structure compared to SMG and DMG devices and hence, hot carrier effect is minimized significantly and a higher breakdown voltage is achieved in TMG architecture. Peaks occurring in electric field profile at the interface of different gate metals result in an increase of average electric field in the channel and enhancement in electron transport velocity as well. Thus, the study lifts up the enhanced performance of the proposed device architecture in terms of suppression of SCEs and improved carrier transport efficiency. Trapping effects, a major limiting factor of device performance, has been analyzed in this work and observed that increase of trapped charge causes reduction in 2DEG density. Along with investigating the areas of improvement, impact of variation in device parameters and bias voltages like individual metal gate length ratio, barrier layer thickness, total channel length, mole fraction of Al, doping density of barrier layer and drain to source voltage on different device characteristics have been thoroughly

examined. The accuracy of the proposed analytical model has been authenticated by matching the results obtained from the numerical simulations. An excellent agreement is observed with a reasonable accuracy over a broad range of device parameters. Quantum Mechanical Effect and Ballistic Transport have not been included in this work because the device dimensions assumed for the modeling are long enough not to cause such effects in a practical device of similar dimensions. Self-heating effect of the device has also been studied by developing a simulation model with the help of commercially available software package. Temperature distribution profile across the device has been explored and compared with the other HEMT structures. Effects of drain voltage and gate voltage on maximum temperature generated during operation have been investigated. It has been observed in the study that though TMG HEMT provides high carrier velocity, temperature increases to an insignificant amount from other structures. This concludes, superior device behavior can be achieved without sacrificing thermal performance with the proposed device structure. However, fabrication of TMG HEMT is a challenging task because of the difficulty associated with depositing three different metals on short gate terminal, however this work inspires the potentials of the device in future nanotechnology.

6.2 Scope of Future Works:

The potential future extensions of the existing work have been listed below:

- Quantum Mechanical Effects (QMEs) have not been considered in our model as the channel length was 120 nm. QMEs become significant at channel lengths below 30 nm. However, it will be interesting to explore the quantum mechanical phenomena in the TMG AlGaN/GaN HEMT device structure with channel length below 30 nm.

- Ballistic transport phenomena have not been considered in our current model because the channel length of the device was 120 nm. Including Ballistic transport phenomena in our model for sub 50 nm device structure will, therefore, be an important scope for future study.

References

[1] Trew, R. J. (2002). SiC and GaN transistors-Is there one winner for microwave power applications?. *Proceedings of the IEEE*, *90 (6)*, 1032–1047.

[2] Ozgur, A., Kim, W., Fan, Z., Botchkarev, A., Salvador, A., Mohammad, S. N., Sverdlov, B. and Morkoc, H. (1995). High transconductance normally-off GaN MODFETs. *Electronics Letters*, *31 (16)*, 1389-1390.

[3] Khan, M.A., Chen, Q., Yang, J.W., Shur, M.S., Dermott, B.T. and Higgins, J.A. (1996). Microwave operation of GaN/AlGaN-doped channel heterostructure field effect transistors. *IEEE Electron Device Letters*, *17(7)*, 325-327.

[4] Gaska, R., Chen, Q., Yang, J., Osinsky, A., Khan, M. A. and Shur, M. S. (1997). High temperature performance of AlGaN/GaN HFETs on SiC substrates*., IEEE Electron Device Letters*, *18(10)*, 492-494.

[5] Wu, Y. F., Keller, S., Kozodoy, P., Keller, B. P., Parish, P., Kapolnek, D., DenBaars, S.P. and Mishra, U. K. (1997). Bias dependent microwave performance of AlGaN/GaN MODFET's up to 100 V. *IEEE Electron Device Letters*, *18(6)*, 290-292.

[6] Ambacher, O., Foutz, B., Smart, J., Shealy, JR., Weimann, NG, Chu, K., Murphy, M., Sierakowski, AJ, Schaff, WJ, Eastman, LF and others. (2000). Two dimensional electron gases induced by spontaneous and piezoelectric polarization in undoped and doped AlGaN/GaN heterostructures. *Journal of applied physics*, *87(1)*, 334-344.

[7] Nguyen, N.X., Micovic, M., Wong, W.S., Hashimoto, P., McCray, L.M., Janke, P. and Nguyen, C. (2000). GaN/AlGaN high electron mobility transistors with f of 110 GHz. *IEEE Trans. Electron Lett*, *36(4)*, 358-359.

[8] Pearton, S.J., Zolper, J.C., Shul, R.J. and Ren, F. (1999). GaN: Processing, defects, and devices. *Journal of applied physics*, *86(1)*, 1-78.

[9] Johnson, J.W., Baca, A.G., Briggs, R.D., Shul, R.J., Monier, C., Ren, F., Pearton, S.J., Dabiran, A.M., Wowchack, A.M., Polley, C.J. and Chow, P.P. (2001). Effect of gate length on DC performance of AlGaN/GaNHEMTs grown by MBE. *Solid-State Electronics*, *45(12)*, 1979-1985.

[10] Awano, Y., Kosugi, M., Kosemura, K., Mimura, T. and Abe, M. (1989). Short-Channel Effects in Subquarter-Micrometer-Gate HEMT's: Simulation and Experiment. *IEEE Trans. Electron Devices*, *36(10)*, 2260-2266.

[11] Long, W., and Chin, K. K. (1997). Dual material gate field effect transistor (DMGFET). In *Electron Devices Meeting, 1997. IEDM'97. Technical Digest., International, IEEE,* 549-552.

[12] Kumar, S. P., Agrawal, A., Chaujar, R., Gupta, M. and Gupta, R. S. (2008). Analytical modeling and simulation of subthreshold behavior innanoscale dual material gate AlGaN/GaN HEMT. *Superlattices and Microstructures*, *44(1)*, 37-53.

[13] Chiang, T. K. (2009). A new two-dimensional analytical subthreshold behavior model for short-channel tri-material gate-stack SOI MOSFET's. *Microelectronics Reliability*, *49(2)*, 113-119.

[14] Dhanaselvama, P. S. and Balamurugana, N. B. (2013). Analytical approach of a nanoscale triple-material surrounding gate (TMSG) MOSFETs for reduced short-channel effects. *Microelectronics Journal*, *44(5)*, 400–404.

[15] Wang, H.K., Wu, S., Chiang, T.K. and Lee, M.S. (2012). A new two dimensional analytical threshold voltage model for short-channel triple-material surrounding-gate metal-oxide-semiconductor field-effect transistors. *Japanese Journal of Applied Physics*, *51(5)*, 4301.

[16] Mahmud, M. A., and Subrina, S. (2016). Two-dimensional analytical model of threshold voltage and drain current of a double-halo gate-stacked triple-material double-gate MOSFET. *Journal of Computational Electronics*, 1-12.

[17] Vanitha, P., Balamurugan, N. B., and Priya, G. L. (2015). Triple Material Surrounding Gate (TMSG) Nanoscale Tunnel FET-Analytical Modeling and Simulation. *Journal Of Semiconductor Technology And Science*, *15*(6), 585-593.

[18] Li, C., Zhuang, Y. and Zhuang, L. (2012). Simulation study on FinFET with tri-material gate. *IEEE International Conference on Electron Devices and Solid State Circuit (EDSSC)*, 1-3.

[19] Khan, M.A., Kuznia, J.N., Olson, D.T., Schaff, W.J., Burm, J.W. and Shur, M.S. (1994). Microwave performance of a 0.25μm gate AlGaN/GaN heterostructure field effect transistor. *Applied Physics Letters*, *65(9)*.

[20] Ambacher, O., Smart, J., Shealy, J. R., Weimann, N. G., Chu, K., Murphy, M., Schaff, W. J., Eastman, L. F., Dimitrov, R., Wittmer, L., Stutzmann, M., Rieger, W. and Hilsenbeck, J. (1999). Two-dimensional electron gases induced by spontaneous and piezoelectric polarization charges in N- and Ga-face AlGaN/GaN heterostructures. *Journal of applied physics*, *85(6)*, 3222-3233.

[21] Tyagi, R.K., Ahlawat, A., Pandeyb, M. and Pandeya, S. (2007). An analytical two-dimensional model for AlGaN/GaN HEMT with polarization effects for high power applications. *Microelectronics journal*, *38*, 877-883.

[22] Kumar, S.P., Agrawal, A., Kabraa, S., Guptaa M. and Guptaa, R.S. (2006). An analysis for AlGaN/GaN modulation doped field effect transistor using accurate velocity-field dependence for high power microwave frequency applications. *Microelectronics journal*, *37*, 1339-1346.

[23] Asbeck, P.M., Yu, E.T., Lau, S.S., Sullivan, G.J., Hove, J.V. and Redwing, J. (1997). Piezoelectric charge densities in AIGaN/GaN HFETs. *Electronics Letters*, *33(14)*, 1230-1231,

[24] Lenka, T.R. and Panda, A.K. (2011). Characteristics Study of 2DEG Transport Properties of AlGaN/GaN and AlGaAs/GaAs-based HEMT. *Semiconductors*, *45(5)*, 650-656.

[25] Zhang, W., Zhang, Y., Mao, W., Ma, X., Zhang, J. and Hao, Y. (2013). Influence of the Interface Acceptor-Like Traps on the Transient Response of AlGaN/GaN HEMTs. *IEEE Electron Device Letters*, *34(1)*, 45-47.

[26] Tirado, J.M., Sanchez-Rojas, J. L. and Izpura, J. I. (2007). Trapping effects in the transient response of AlGaN/GaN HEMT devices. *IEEE Trans. Electron Devices*, *54(3)*, 410–417.

[27] Bradley, S. T., Young, A. P., Brillson, L. J., Murphy, M. J., Schaff, W. J., and Eastman, L. F. (2001). Influence of AlGaN deep level defects on AlGaN/GaN 2-DEG carrier confinement. *IEEE Trans. Electron Devices*, *48(3)*, 412-415.

[28] Klein, P. B., and Binari, S. C. (2003). Photoionization spectroscopy of deep defects responsible for current collapse in nitride-based field effect transistors. *Journal of Physics: Condensed Matter*, *15(44)*, R1641.

[29] Binari, S.C., Ikossi, K., Roussos, J.A., Kruppa, W., Park, D., Dietrich, H.B., Koleske, D.D., Wickenden, A.E. and Henry, R.L. (2001). Trapping effects and microwave power performance in AlGaN/GaN HEMTs. *IEEE Trans. Electron Devices*, *48(3)*, 465-471.

[30] Chattopadhyay, M. K. (2008). Thermal model for AlGaN/GaN HEMTs including self-heating effect and non-linear polarization. *International Conference on Recent Advances in Microwave Theory and Applications*.

[31] Hosch, M., Pomeroy, J. W., Sarua, A., Kuball, M., Jung, H., and Schumacher, H. (2009). Field dependent self-heating effects in high-power AlGaN/GaN HEMTs. In *Proc. CS MANTECH Conf.*, 32-55.

[32] Ahmad, I., Kasisomayajula, V., Song, D. Y., Tian, L., Berg, J. M., and Holtz, M. (2006). Self-heating in a GaN based heterostructure field effect transistor: Ultraviolet and visible Raman measurements and simulations. *Journal of applied physics*, *100(11)*, 113718.

[33] Gaska, R., Osinsky, A., Yang, J. W., and Shur, M. S. (1998). Self-heating in high-power AlGaN-GaN HFETs. *IEEE Electron Device Letters*, *19(3)*, 89-91.

[34] Wu, Y. R., & Singh, J. (2007). Transient study of self-heating effects in AlGaN/GaN HFETs: Consequence of carrier velocities, temperature, and device performance. *Journal of applied physics*, *101(11)*, 113712.

[35] Awano, Y., Kosugi, M., Mimura, T., & Abe, M. (1987). Performance of a quarter-micrometer-gate ballistic electron HEMT. *IEEE Electron Device Letters*, *8(10)*, 451-453.

[36] Chen, C. H., Coffie, R., Krishnamurthy, K., Keller, S., Rodwell, M., and Mishra, U. K. (2000). Dual-gate AlGaN/GaN modulation-doped field-effect transistors with cut-off frequencies f T> 60 GHz. *IEEE Electron Device Letters*, *21(12)*, 549-551.

[37] Palacios, T., Chakraborty, A., Heikman, S., Keller, S., DenBaars, S. P., and Mishra, U. K. (2006). AlGaN/GaN high electron mobility transistors with InGaN back-barriers. *IEEE Electron Device Letters*, *27(1)*, 13-15.

[38] Shur, M. (1989). Split-gate field-effect transistor. *Applied Physics Letters*, *54(2)*, 162-164.

[39] Ismail, K., Lee, K. Y., Kern, D. P., and Hong, J. M. (1990). Novel properties of a 0.1-mu m-long split-gate MODFET. *IEEE Electron Device Letters*, *11(10)*, 469-471.

[40] del Alamo, J. A., and Joh, J. (2009). GaN HEMT reliability. *Microelectronics reliability*, *49(9)*, 1200-1206.

[41] Sumiya, M., and Fuke, S. (2004). Review of polarity determination and control of GaN. *MRS Internet Journal of Nitride Semiconductor Research*, *9*, e1.

[42] Rivera, C., and Munoz, E. (2009). The role of electric field-induced strain in the degradation mechanism of AlGaN/GaN high-electron-mobility transistors. *Applied Physics Letters*, *94(5)*, 053501.

[43] Joh, J., and Del Alamo, J. A. (2008). Critical voltage for electrical degradation of GaN high-electron mobility transistors. *IEEE Electron Device Letters*, *29(4)*, 287-289.

[44] Mishra, U. K., Parikh, P., and Wu, Y. F. (2002). AlGaN/GaN HEMTs-an overview of device operation and applications. *Proceedings of the IEEE*, *90(6)*, 1022-1031.

[45] Foutz, B. E., O'Leary, S. K., Shur, M. S., and Eastman, L. F. (1999). Transient electron transport in wurtzite GaN, InN, and AlN. *Journal of Applied Physics*, *85(11)*, 7727-7734.

[46] Siklitsky, V., Tolmatchev, A., Bougrov, V., Levinshtein, M. E., Rumyanstev, S., and Zubrilov, A. (2005). Electronic archive new semiconductor materials. Characteristics and properties. *IOFFE Physicotechnical Institut*.

[47] Tolbert, L. M., Ozpineci, B., Islam, S. K., and Chinthavali, M. S. (2003). Wide bandgap semiconductors for utility applications. S*emiconductors*, *1*, 3.

[48] Binari, S. C., Rowland, L. B., Kruppa, W., Kelner, G., Doverspike, K., and Gaskill, D. K. (1994). Microwave performance of GaN MESFETS. *Electronics letters*, *30(15)*, 1248-1249.

[49] Trivedi, M., and Shenai, K. (1999). Performance evaluation of high-power wide band-gap semiconductor rectifiers. *Journal of Applied Physics*, *85(9)*, 6889-6897.

[50] Daumiller, I., Kirchner, C., Kamp, M., Ebeling, K. J., and Kohn, E. (1999). Evaluation of the temperature stability of AlGaN/GaN heterostructure FETs. *IEEE Electron Device Letters*, *20(9)*, 448-450.

[51] Ionascut-Nedelcescu, A., Carlone, C., Houdayer, A., Von Bardeleben, H. J., Cantin, J. L., and Raymond, S. (2002). Radiation hardness of gallium nitride. *IEEE Trans. Nuclear Science*, *49(6)*, 2733-2738.

[52] Stutzmann, M., Ambacher, O., Eickhoff, M., Karrer, U., Lima Pimenta, A., Neuberger, R., Schalwig, J., Dimitrov, R., Schuck, P.J. and Grober, R.D. (2001). Playing with polarity. *physica status solidi (b)*, *228(2)*, 505-512.

[53] Faqir, M., Verzellesi, G., Chini, A., Fantini, F., Danesin, F., Meneghesso, G., Zanoni, E. and Dua, C. (2008). Mechanisms of RF current collapse in AlGaN–GaN high electron mobility transistors. *IEEE Trans. Device and Materials Reliability*, *8(2)*, 240-247.

[54] Morkoc, H. (2008). Handbook of Nitride Semiconductors and Devices*, 1*. *Wiley-vch*.

[55] Jarndal, A. H. (2006). Large Signal Modeling of GaN Device for High Power Amplifier Design. *kassel university press GmbH*.

[56] Macfarlane, D. J. (2014). *Design and fabrication of AlGaN/GaN HEMTs with high breakdown voltages.* (Doctoral dissertation, University of Glasgow).

[57] Sarua, A., Ji, H., Kuball, M., Uren, M.J., Martin, T., Nash, K.J., Hilton, K.P. and Balmer, R.S. (2006). Piezoelectric strain in AlGaN⁄ GaN heterostructure field-effect transistors under bias. *Applied physics letters*, *88(10)*, 103502.

[58] Jogai, B. (2003). Influence of surface states on the two-dimensional electron gas in AlGaN/GaN heterojunction field-effect transistors. *Journal of applied physics*, *93(3)*, 1631-1635.

[59] Gordon, L., Miao, M. S., Chowdhury, S., Higashiwaki, M., Mishra, U. K., & Van de Walle, C. G. (2010). Distributed surface donor states and the two-dimensional electron gas at AlGaN/GaN heterojunctions. *Journal of Physics D: Applied Physics*, *43(50)*, 505501.

[60] Ibbetson, J. P., Fini, P. T., Ness, K. D., DenBaars, S. P., Speck, J. S., and Mishra, U. K. (2000). Polarization effects, surface states, and the source of electrons in AlGaN/GaN heterostructure field effect transistors. *Applied Physics Letters*, *77(2)*, 250-252.

[61] Karmalkar, S., Shur, M. S., and Gaska, R. (2003). GaN-based power high electron mobility transistors. *Wide Energy Bandgap Electronic Devices*, 173-213.

[62] Meneghesso, G., Verzellesi, G., Pierobon, R., Rampazzo, F., Chini, A., Mishra, U.K., Canali, C. and Zanoni, E. (2004). Surface-related drain current dispersion effects in AlGaN-GaN HEMTs. *IEEE Trans. Electron Devices*, *51(10)*, 1554-1561.

[63] Klein, P. B., Binari, S. C., Ikossi-Anastasiou, K., Wickenden, A. E., Koleske, D. D., Henry, R. L., and Katzer, D. S. (2001). Investigation of traps producing current collapse in AlGaN/GaN high electron mobility transistors. *Electronics Letters*, *37(10)*, 1.

[64] Sadi, T., Kelsall, R. W., and Pilgrim, N. J. (2006). Investigation of Self-Heating Effects in Submicrometer GaN/AlGaN HEMTs Using an Electrothermal Monte Carlo Method. *IEEE Trans. Electron Devices*, *53(12)*, 2892-2900.

[65] Xing, H., Keller, S., Wu, Y.F., McCarthy, L.,Smorchkova, I.P., Buttari, D., Coffie, R., Green, D.S., Parish, G., Heikman, S. and Shen, L. (2001). Gallium Nitride Based Transistors. *Journal of Physics: Condensed Matter*, *13(32)*, 7139-7157.

[66] Borges, R. (2005). High Electron Mobility Transistors (HEMT)." internet.

[67] Kumar, S.P., Agrawal, A., Chaujar, R., Kabra, S., Gupta, M. and Gupta, R.S. (2007). Threshold voltage model for small geometry AlGaN/GaN HEMTs based on analytical solution of 3-D Poisson's equation. *Microelectronics Journal*, *38(10)*, 1013-1020.

[68] DasGupta, N., DasGupta, A. (1993). An analytical expression for sheet carrier concentration vs gate voltage for HEMT modeling. *Solid-State Electronics*, *36(2)*, 201-203.

[69] Chattopadhyay, M.K. and Tokekar, S. (2006). Temperature and polarization dependent polynomial based non-linear analytical model for gate capacitance of $Al_mGa_{1-m}N$/GaNMODFET. *Solid-State Electronics*, *50(2)*, 220-227.

[70] Robin, P. and Rohdin, H. (2002). *High Speed Heterostructure Devices: From Device Concepts to Circuit Modeling*. Cambridge University Press.

[71] Silvaco International, "Silvaco International, ATLAS User's Manual, February 2000." (2000).

[72] Trew, R. J., Green, D. S., & Shealy, J. B. (2009). AlGaN/GaN HFET reliability. *Microwave Magazine, IEEE*, *10(4)*, 116-127.

[73] Benbakhti, B., Soltani, A., Kalna, K., Rousseau, M. and De Jaeger, J.-C. (2009). Effects of Self-Heating on Performance Degradation in AlGaN/GaN-Based Devices. *IEEE Trans. Electron Devices*, *56(10)*, 2178–2185.

[74] Benbakhti, B., Rousseau, M., and De Jaeger, J-C. (2005). Implementation of an 2D Electro-Thermal Model for Power Semiconductor Devices Simulation: Application on Gallium Nitride. *Proceedings of the COMSOL Users Conference*, Paris, France.

[75] Millett, R., Wheeldon, J., Hall, T., and Schriemer, H. (2006). Towards Modelling Semiconductor Heterojunctions. *Proceedings of the COMSOL Users Conference*, Boston, MA.